Atlantic Tropical Cyclone Activity in Response to the MJO in NOAA's CFS Model

ANTHONY G. BARNSTON AND NICOLAS VIGAUD

International Research Institute for Climate and Society, Columbia University, Palisades, New York

LINDSEY N. LONG

NOAA/Climate Prediction Center, College Park, and Innovim, LLC, Greenbelt, Maryland

MICHAEL K. TIPPETT

International Research Institute for Climate and Society, Columbia University, Palisades, New York, and Center of Excellence for Climate Change Research, Department of Meteorology, King Abdulaziz University, Jeddah, Saudi Arabia

JAE-KYUNG E. SCHEMM

NOAA/Climate Prediction Center, College Park, Maryland

(Manuscript received 3 April 2015, in final form 16 July 2015)

ABSTRACT

The Madden–Julian oscillation (MJO) is known to exert some control on the variations of North Atlantic tropical cyclone (TC) activity within a hurricane season. To explore the possibility of better TC predictions based on improved MJO forecasts, retrospective hindcast data on MJO and on TC activity are examined both in the current operational version of the CFSv2 model (T126 horizontal resolution) and a high-resolution (T382) experimental version of CFS. Goals are to determine how well each CFS version reproduces reality in 1) predicting MJO and 2) reproducing observed relationships between MJO phase and TC activity. For the operational CFSv2, skill of forecasts of TC activity is evaluated directly.

Both CFS versions reproduce MJO behavior realistically and also roughly approximate observed relationships between MJO phase and TC activity. Specific biases in the high-resolution CFS are identified and their causes explored. The high-resolution CFS partially reproduces an observed weak tendency for TC activity to propagate eastward during and following the high-activity MJO phases. The operational (T126) CFSv2 shows useful skill (correlation >0.5) in predicting the MJO phase and amplitude out to ~3 weeks. A systematic error of slightly too slow MJO propagation is detected in the operational CFSv2, which still shows usable skill (correlation >0.3) in predicting weekly variations in TC activity out to 10–14 days. A conclusion is that prediction of intraseasonal variations of TC activity by CFSv2 is already possible and implemented in real-time predictions. An advantage of the higher resolution in the T382 version is unable to be confirmed.

1. Introduction

The activity[1] level of a season of Atlantic tropical cyclones (TC) is controlled by numerous known influences (e.g., Klotzbach 2007). Additionally, variations of activity within a season are under the control of several factors. One such factor is the Madden–Julian oscillation (MJO), which is an eastward propagating disturbance focused largely in the tropical atmosphere but with influences outside the tropics (Madden and

[1] We use "activity" as a general term that may be applied to the number of tropical cyclones per unit of time, their integrated intensity, or instances of genesis or rapid intensification. Distinctions among these aspects are made later.

Denotes Open Access content.

Corresponding author address: Anthony G. Barnston, Monell Building, IRI, 61 Route 9W, Palisades, NY 10964.
E-mail: tonyb@iri.columbia.edu

DOI: 10.1175/MWR-D-15-0127.1

© 2015 American Meteorological Society

Julian 1994; Jones et al. 2004). Atlantic TC activity has been associated with the MJO in a number of studies. Maloney and Hartmann (2000) noted a strong preference for tropical cyclone genesis in the Gulf of Mexico and the Caribbean during times of anomalous westerly low-level wind in the eastern tropical Pacific. Westerly wind anomalies are associated with MJO phases 8, 1, and 2, versus easterly anomalies with phases 4, 5, and 6, respectively, in the system later developed by Wheeler and Hendon (2004). Somewhat similarly, Mo (2000) found activity in the North Atlantic to be generally enhanced during MJO phases 1 and 2 (when convection is enhanced over eastern Africa and the Indian Ocean) and suppressed during phases 6 and 7 (with enhanced convection over the Pacific Ocean). These observed relationships between MJO and eastern Pacific and Atlantic TCs were further supported and expanded by Higgins and Shi (2001), where enhanced convection as well as TC genesis was noted just to the east of the region having low-level westerly wind anomalies. The general findings of greater Atlantic TC activity during MJO phases 1 and 2, and lesser activity in phases 6 and 7, were later replicated in Klotzbach (2010) and extended specifically to cases of rapid TC intensification in Klotzbach (2012), where environmental factors such as vertical shear and relative humidity were suggested as physical bases for the MJO influence on TC development.

An important role of African easterly waves in the intraseasonal variation of Atlantic TC activity was indicated in Ventrice et al. (2011), where the MJO is seen to influence not only heightened African convection and the attendant Atlantic TC-enhancing easterly waves but also the larger-scale tropical and subtropical North Atlantic environmental factors such as vertical wind shear, low-level vorticity, and atmospheric moisture, the net result being further enhanced Atlantic TC activity observed during MJO phases 1, 2, and 3.

The observed relationship between the MJO and Atlantic TC activity has been supported in dynamical model studies, which help identify the pertinent physical mechanisms. The MJO itself has been characterized as a disturbance whose eastward propagation is propelled by a convection-enhancing eastward-moving Kelvin wave on the east side of the current MJO region and a convection-eroding westward-moving Rossby wave on the west side (Matthews 2000). The MJO was identified as a coupled ocean–atmosphere phenomenon in Matthews (2004), where the region of enhanced convection occurs as a lagged response to an MJO-related warming of underlying sea surface temperature in the Hadley Centre Atmosphere Model, version 3 (HadAM3). A case study involving the MJO and tropical cyclogenesis in the Indian Ocean showed successful reproduction of an observed TC by the UH_HCM model of the University of Hawaii, partly as a result of skillful MJO forecasts (Fu and Hsu 2011). Using the ECMWF Monthly Forecast System (ECMFS), Belanger et al. (2010) showed that when the MJO-related enhanced convection is in the Indian Ocean (e.g., during MJO phases 1, 2, and 3) there are skillful predictions of heightened likelihood of TC activity in the Gulf of Mexico, the Caribbean, and other parts of the North Atlantic. These skillful forecasts were related to the model's ability to reproduce enhanced low-level relative vorticity, reduced vertical shear, and increased frequency of African easterly waves. A similar result using the ECMWF model had earlier been produced by Vitart (2009), where midlevel relative humidity was also identified as a pivotal environmental variable.

Here we explore the capability of the NOAA Climate Forecast System (CFS) coupled model to reproduce not only MJO behavior itself, but the observed effects of the MJO on Atlantic TCs. We analyze retrospective hindcasts both from the current operational version of CFSv2 (with T126 horizontal resolution), and from a high-resolution (T382, or 38 km) version of CFS to investigate the realism of each version, and learn whether the higher resolution provides a better semblance of reality.

2. Data and methods

The U.S. National Oceanic and Atmospheric Administration (NOAA)/Climate Prediction Center (CPC) provided the MJO-constituent data from the current operational T126 horizontal-resolution CFS v2 (approximately 94 km, referred to as the CFSv2) (Saha et al. 2014). The CFSv2 is a fully coupled atmosphere–ocean–land system. The Global Forecast System (GFS) is coupled to the GFDL Modular Ocean Model 4 (MOM4) and Noah land surface model. CFSv2 hindcasts were supplied for 45-day lead times initialized every 6 h from 1999 to 2010. This model output data includes 850-hPa height, 200-hPa height, and outgoing longwave radiation (OLR) needed for MJO phase and amplitude diagnosis. NOAA/CPC also provided Atlantic TC tracks and four-times-daily TC characteristics—maximum wind speed and minimum pressure, using the TC detection and tracking methods described in Camargo and Zebiak (2002). This detection method requires a grid point to meet seven criteria to be considered a TC. The grid point must be a warm core system, a minimum in sea level pressure, have wind speeds stronger at 850 than at 300 hPa, and surpass model- and basin-dependent thresholds for 850-hPa vorticity, vertically integrated temperature anomaly, and surface wind speed. The grid point is then tracked forward and backward in time using a relaxed

vorticity threshold of $3.5 \times 10^{-5}\,s^{-1}$. Because a higher horizontal resolution is used here than in Camargo and Zebiak (2002), the tracking box is extended from 3×3 grid boxes to 5×5 grid boxes. The accumulated cyclone energy (ACE) index is derived by summing the squares of the maximum wind speeds across all active TCs every 6 h. Observed TC data during the same 12-yr period is taken from the NOAA/National Hurricane Center Best Track Hurricane Database (HURDAT) (Landsea et al. 2004).

NOAA/CPC additionally provided the same data fields, including TC tracks and characteristics, for hindcast runs with a high-resolution version of CFS at T382 spatial resolution (approximately 38 km, referred to as the T382 CFS) over the period 1981–2008. This dataset consists of five ensemble members initialized on five days (10, 12, 14, 16, and 18) in April, run through the end of November of each year. Note that this mid-April initialization serves as the only initialization for each year, unlike the CFSv2 that is initialized four times daily throughout each calendar year. This model was run as an experimental version of CFS and therefore differs slightly from the operational CFSv2. Besides the higher resolution, the seasonal T382 CFS also uses MOM3 as its ocean component versus the MOM4, which is used in the operational CFSv2.

For the T382 CFS, software was created to diagnose the phase and amplitude of the MJO following the protocol in Wheeler and Hendon (2004), using upper (200 hPa) and lower (850 hPa) level wind and outgoing longwave radiation (OLR) data.[2] First, the mean and the first three harmonics are removed to eliminate the annual cycle. Next, to remove variability on the interannual time scale (e.g., ENSO effects), the mean of the 120 days prior to the day in question is removed. However, because T382 CFS model output is not available before late April, for days early in the season part or all of the 120-day mean is derived from Reanalysis-2 observations (Kanamitsu et al. 2002) after a regression-based removal of the association with the ENSO-related Niño-3.4 (Barnston et al. 1997) sea surface temperature (SST) anomalies. Here the Niño-3.4 SST index takes the place of the first rotated empirical orthogonal function (EOF) of Indo-Pacific SST, which was used in Wheeler and Hendon (2004). Finally, using EOF analysis, the Real-time Multivariate MJO (RMM) time series for the first and second EOFs (RMM1 and RMM2) of the MJO state are defined, leading to calculations of the model's MJO amplitude and phase.

For the operational CFSv2, the MJO state was defined slightly differently, using the method of Wang et al. (2014). Here, after removing the annual cycle using the mean and the first 3 harmonics, the daily anomalies are then filtered using a 20–100-day bandpass filter.[3] This method to remove interannual variability differs from the Wheeler and Hendon (2004) method in that a regression with respect to an ENSO-related time series is not used, but rather the direct application of the bandpass filter to the variable of interest. In the operational CFSv2, the MJO "observation" of MJO is constructed from the RMM1 and RMM2 of the CFSv2 initial conditions (i.e., the "forecast" at lead zero, benefitting from the data assimilation) using this Wang et al. (2014) method. The correlation with the corresponding observation from Wheeler and Hendon (2004) is 0.93, indicating high consistency between the two versions of MJO observation.

3. Results

a. T382 CFS

We first discuss results for the T382 CFS, which consists of five ensemble members run for each hurricane season (May to November) of each year, initialized on five days in April of the respective year. Here the prediction-determining information in the initial conditions is lost in 2–3 weeks, so that the runs are useful primarily in diagnosing the realism of the model's Atlantic TC behavior relative to its MJO state.

1) BASINWIDE MJO INFLUENCE

We explore the degree of realism of the model's TC activity in relation to its MJO phase as represented by four variables: 1) the number of TCs, 2) ACE, 3) instances of genesis (first appearance of a TC), and 4) instances of rapid intensification of a TC [an increase of at least 10 kt ($5.1\,m\,s^{-1}$) in a 6-h period]. For the above variables, a TC is defined when the maximum wind speed is at least that of a tropical storm, at 34 kt ($17.5\,m\,s^{-1}$). Using the tracking algorithm described above, only a small percentage of cyclones are below this threshold and considered tropical depressions; therefore, no model scaling was deemed necessary. The relative frequencies of each of these four variables as a function of MJO phase, normalized by time spent in each phase, are shown in Fig. 1 for the observations and for the T382 CFS. Figure 1 shows that to first order, the model TC activity is greatest in MJO phases 1 and 2 and

[2] It should be noted that the MJO can also be defined using 200-hPa velocity potential in place of OLR, as illustrated in Ventrice et al. (2013).

[3] The Wang et al. (2014) method could not be applied to the T382 CFS model because the output data begin only in mid-April of each year.

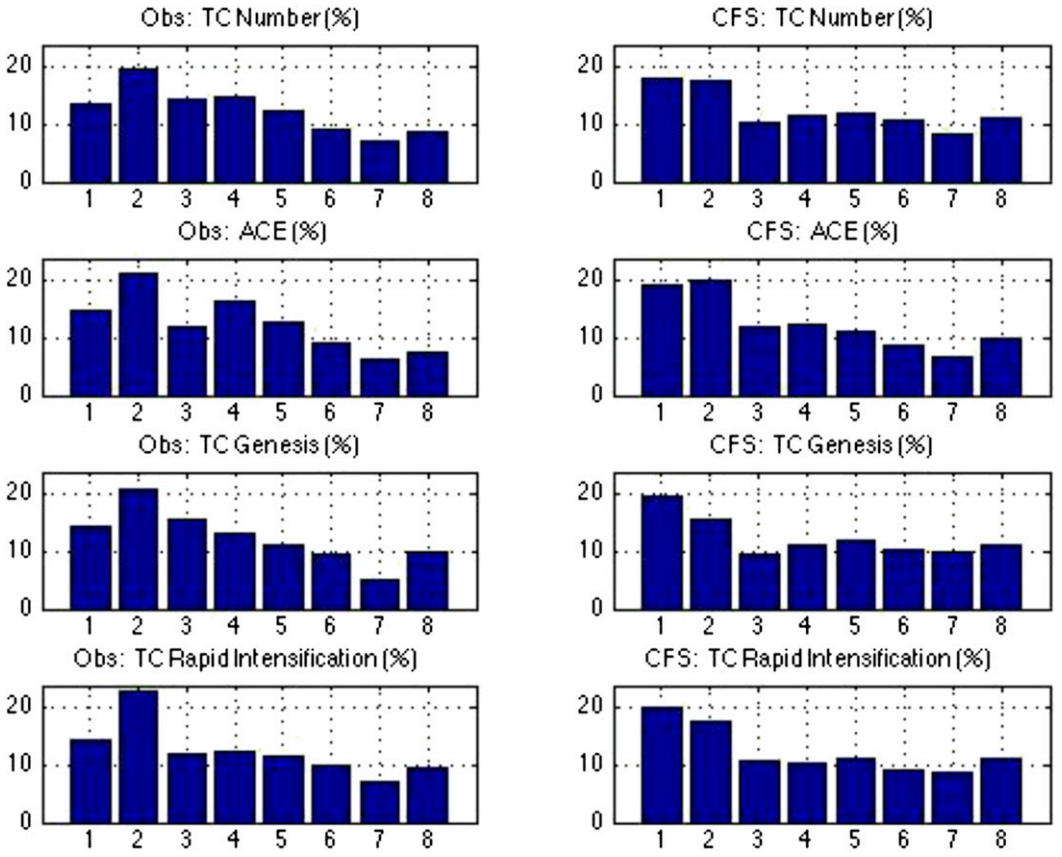

FIG. 1. Percentage distribution of Atlantic hurricane activity by MJO phase for (left) observations and for (right) the T382 CFS model for (top) number of storms, (second from top) accumulated cyclone energy, (second from bottom) storm genesis, and (bottom) instances of rapid intensification. The data are normalized by time spent in each MJO phase. Correlation between the observed and model patterns over the eight MJO phases are 0.71, 0.87, 0.52, and 0.76, respectively.

is relatively lower in phases 6 and 7, both roughly in keeping with the observations. The correlations between the model and observed activity over the eight MJO phases is in the 0.70s and 0.80s (see Fig. 1 caption), although for genesis it is only 0.52. The correlation for ACE is highest likely because it accounts for TC activity in a strength-inclusive manner, as opposed to the discrete nature of the other three TC variables that renders them more sensitive to sampling variability. We conclude that the relationship between MJO and TC activity is generally reproduced in the T382 CFS model. Discrepancies may be due to either or both of model imperfections and sampling error—particularly in view of the observed data having just one ''ensemble member'' over the 28-yr period. In the next subsection, the observed and modeled spatial distributions of TC activity within the North Atlantic is examined in greater detail, and some large-scale environmental fields are viewed to better understand the findings.

2) NONUNIFORMITY OF MJO INFLUENCE ACROSS SUBSECTORS

In addition to preferential basinwide TC activity for some MJO phases over others, we examine the extent to which these overall preferences apply uniformly to the subsectors of the North Atlantic. The alternative would be preferences that differ by subsector, in which certain subsectors are particularly favored for activity as a function of MJO phase in the observations and, hopefully, in a similar manner in the T382 CFS model. A tendency for some subsectors to have more TC activity than others as a function of MJO phase might be expected if the influence of MJO on TC activity propagated from west to east in parallel with the propagation of the MJO itself. However, the expectation of a west-to-east influence is not necessarily straightforward, because an MJO influence has been suggested to come not only from the MJO's general eastward movement, but also in part from westward propagating equatorial Rossby waves (Matthews 2000)

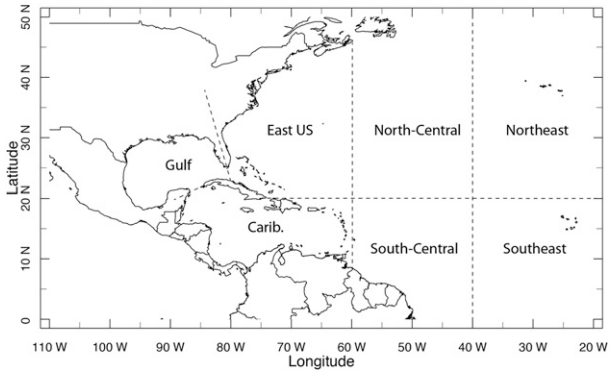

FIG. 2. The seven subsectors of the North Atlantic basin.

and westward-moving African easterly waves (Ventrice et al. 2011; Belanger et al. 2010; Ventrice and Thorncroft 2013) and the TCs themselves at tropical latitudes, within the broader region of the MJO influence. For this analysis we focus mostly on ACE, as it produces the strongest MJO–TC relationships among the four TC variables in most of our analyses.

To examine the dependence of TC activity on MJO phase in more spatial detail, we divide the North Atlantic basin into seven subsectors, as shown in Fig. 2. The subsectors over open ocean are defined using rectangular boundaries, but the Gulf, Caribbean, and eastern U.S. regions conform to their geographical boundaries. Table 1 shows the percentage of total TC activity in each of the seven subsectors for TC number and for ACE, for the observations, and for the T382 CFS model. The model produces proportionately less activity than observations in the Gulf of Mexico for both TC number and ACE and less activity in the Caribbean and the eastern United States for ACE. The model's somewhat low proportion of activity in these subsectors is counterbalanced by greater than the observed proportion of activity in the southeastern part of the North Atlantic basin.

Figure 3 shows the geographical distribution of ACE over the tropical and North Atlantic for MJO phase 2 (a phase of high activity) and phase 7 (a phase of low activity). The difference in observed activity between the two MJO phases is clearly represented in the model output, and the general locations of the observed activity are also approximately reproduced by the model during the 1981–2008 period. However, the southeastward bias in model TC activity mentioned above (Table 1) appears in Fig. 3 as the model underrepresents activity in the Gulf of Mexico in phase 2 and overestimates activity in the southeastern part of the domain in both phases 2 and 7.

This southeastward bias in model TC activity is found to be related to the model's vertical wind shear climatology, which in prior studies of CFS has been found stronger than observed over eastern North America and the western subtropical North Atlantic (not shown). Thus, model TC activity tends to be suppressed in the western/southwestern part of the study domain compared with observations. Related to this climatological shear bias, the T382 CFS is found to have an eastward shift of the climatological upper atmospheric trough position over the continental United States, causing TC trajectories to curve northward and then eastward over the open ocean rather than reaching locations farther west before curving (Fig. 3).

To better understand the nature of the biases in TC activity both generally and as a function of MJO phase, we examine the large-scale patterns of anomalous OLR and zonal wind shear in the tropics and northern subtropics. Figures 4 and 5 show the spatial distributions of observed and T382 CFS model anomalous OLR as a function of MJO phase for the May–November period during the 1981–2008 study period. The observed OLR anomalies roughly agree with the comparable analysis in Wheeler and Hendon (see their Figs. 8 and 9), although their analyses omitted most of the Atlantic. The model results closely resemble those observed, with the strongest OLR anomalies near 10°N latitude.[4] In the Gulf of Mexico, the Caribbean, and the western subtropical North Atlantic, the observations show a slightly negative OLR anomaly (above-average convection) during MJO phases 8, 1, and 2, and the model shows a similar pattern but with slightly stronger anomalous convection in the southeast North Atlantic during phases 1 and 2. This small model difference in the spatial distribution of anomalous OLR is consistent with the biases highlighted above and is consistent with the suspected eastward bias in model climatology of the trough and ridge (i.e., "Bermuda high") positions during the Northern Hemisphere warm season (not shown).

Figure 6 shows the pattern of anomalous 200–850-hPa zonal wind shear in the T382 CFS as a function of MJO phase.[5] Model shear anomaly is most negative in the tropical and subtropical North Atlantic during MJO phases 1, 2, and 3, providing evidence of a critical large-scale

[4] The strongest MJO-induced convection anomalies are expected to be slightly north of the equator during the Northern Hemisphere warm season, consistent with the location of the intertropical convergence zone.

[5] Here, the shear anomaly is for the vector shear, not the magnitude of the shear. Because most of the North Atlantic region of concern has a westerly background shear (except a small region near western Africa, related to the West African monsoon circulation), a reduced shear means less westerly shear—that is, a more favorable environment for TC genesis and growth.

TABLE 1. Percentage of total TC activity in each of the seven subsectors of the North Atlantic Ocean as defined in Fig. 2. Percentages across each row sum to 100. Activity is shown for the observations and for the T382 CFS for each of the two TC variables: TC number and ACE.

		Gulf	Caribbean	Eastern United States	South-central	North-central	Southeast	Northeast
TC No.	Obs	14.4	13.9	24.6	12.1	18.3	8.2	8.5
	382CFS	6.0	13.0	14.5	13.5	16.6	28.0	8.4
ACE	Obs	12.5	15.3	25.9	12.4	21.9	5.2	6.8
	382CFS	3.8	9.6	18.3	15.1	22.5	22.1	8.6

environmental facilitator of enhanced TC activity during those phases. However, the northern boundary of the decreased shear lies at 15°–20°N, which is slightly farther south than observed northern boundary near 22°–25°N (e.g., Figs. 3b and 3c in Klotzbach 2010), extending just north of the northern boundary of the main development region (MDR) at 20°N. The reduced northerly reach of the reduced shear region, particularly during the active MJO phases but also in the model climatology (not shown), is expected to create a model environment less conducive to long, northward-reaching TC paths as they move west-northwestward to the north of the MDR into regions such as the Gulf of Mexico or the waters off the southeast coast of the United States. An analysis for the 850-hPa zonal wind anomaly alone (not shown) is highly similar to the anomalous shear result in the tropical

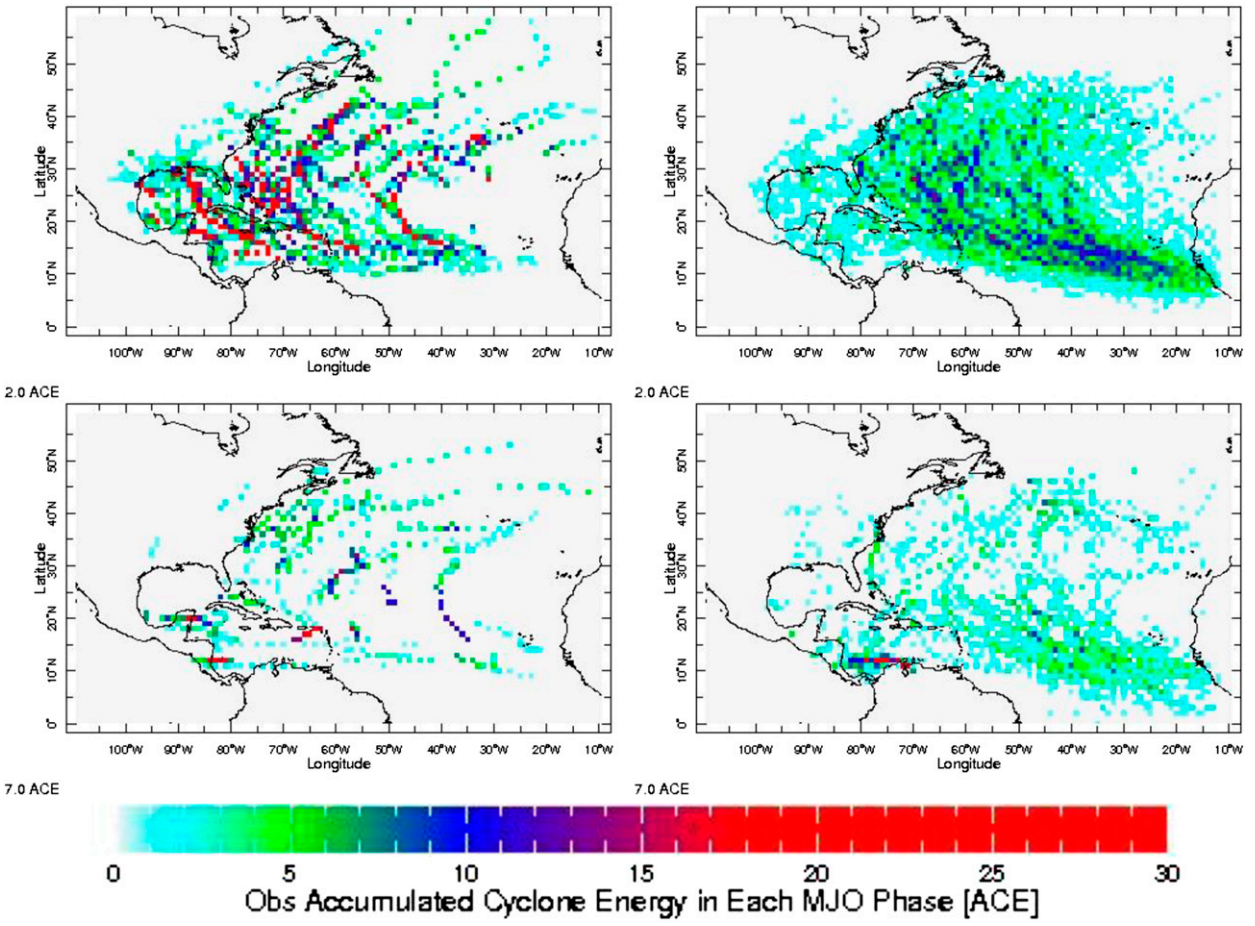

FIG. 3. Atlantic tropical cyclone activity, represented by storm ACE in (left) the observations and in (right) the T382 CFS model. ACE during (top) phase 2 of the MJO, and (bottom) during phase 7. Cyclone energy is accumulated not over the lifetime of a TC but, rather, for each grid cell during the given MJO phase. Five members of CFS model are initialized in mid-April of each year.

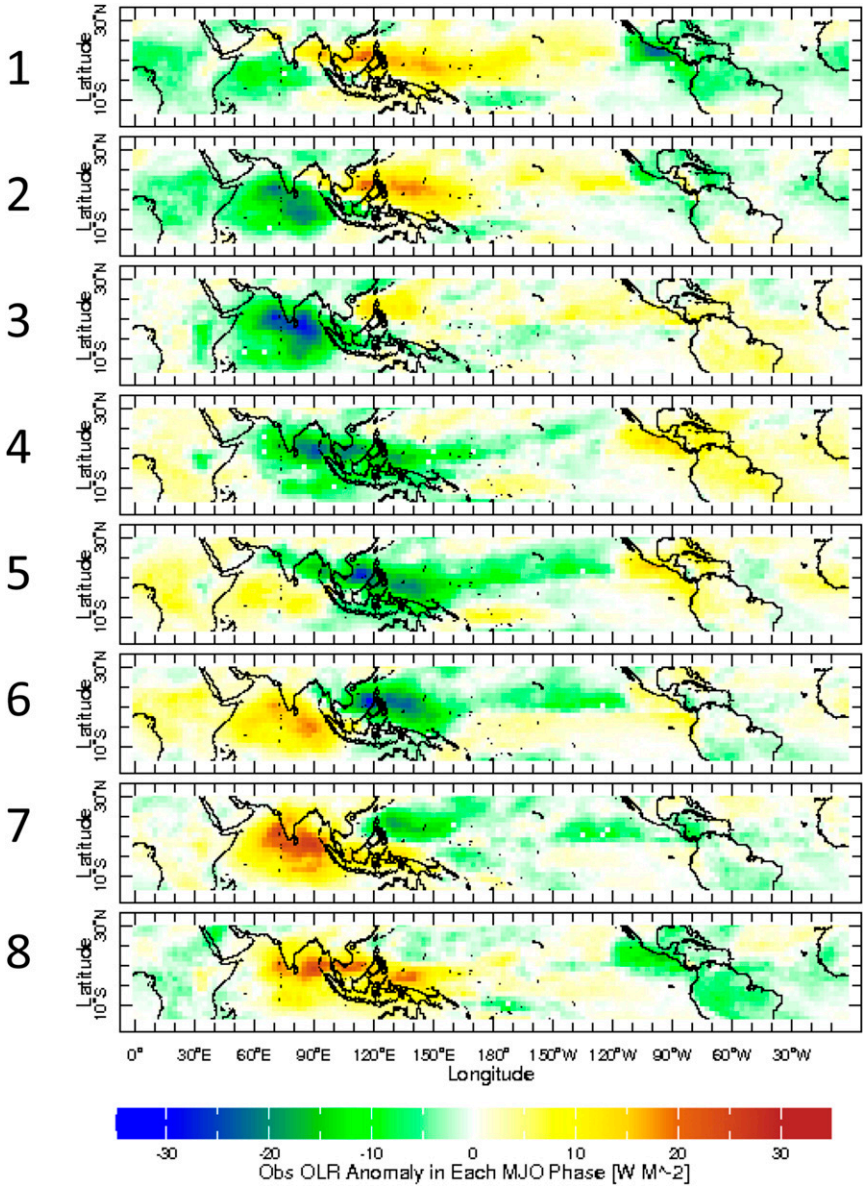

FIG. 4. Observed anomalous outgoing longwave radiation (W m^{-2}) during the days of each of the eight MJO phases during May–November of 1981–2008. Anomalies are defined with respect to the climatologies covering the 28 years for each of the 214 days in the 7-month season.

and subtropical North Atlantic and also shows a westerly low-level wind anomaly matching that observed in the eastern tropical Pacific during MJO phases 8, 1, and 2, as noted in Maloney and Hartmann (2000).

The correlation between observed and model TC activity over the eight MJO phases is shown in Table 2 for individual subsectors, for TC number, and ACE. Most of the correlations are weaker than those found for the North Atlantic basin as a whole, and correlations are higher in the northern tier of sectors than in the southern three sectors. The lack of significant correlation in these tropical sectors implies low reproducibility of TC genesis. In fact, correlations for both genesis and rapid intensification variables are generally only low to moderate (not shown).

To what extent do subsector variations in TC activity parallel those of the Atlantic basin as a whole? Table 3 shows correlations between the ACE in each of the subsectors and that in the entire Atlantic basin, over the eight MJO phases, for the observations and T382 CFS model. The generally high correlations imply subsector behavior paralleling that of the overall Atlantic

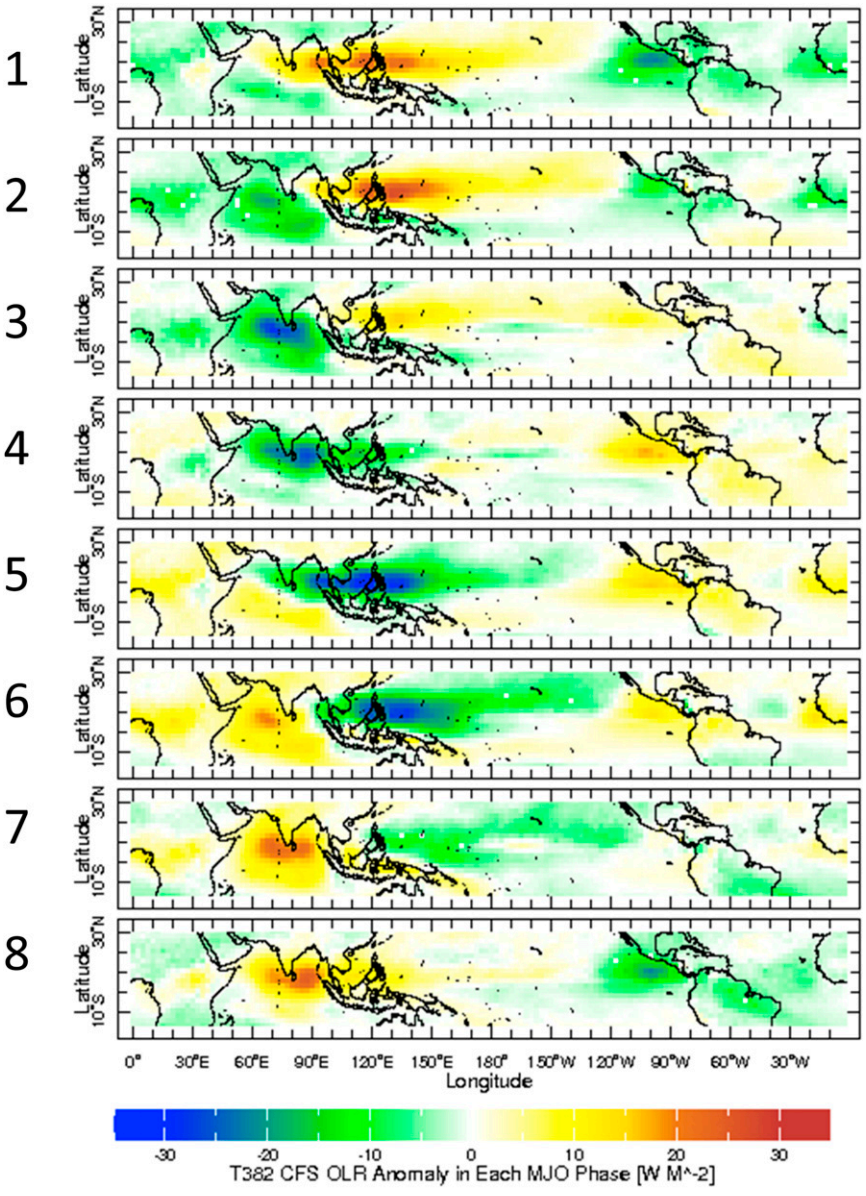

FIG. 5. Anomalous outgoing longwave radiation (W m^{-2}) in the T382 CFS model during the days of each of the model's eight MJO phases during May–November of 1981–2008. Anomalies are defined with respect to the model climatologies covering the 28 years for each of the 214 days in the 7-month season.

basin fairly well and more closely in the model than in the observations. Activity in the eastern U.S. sector appears to be closely associated with overall basin activity, while the variability in the Caribbean appears to be somewhat less so than the other regions, particularly in the model. Although these correlations cannot rule out a possible eastward propagation of enhanced TC activity, they suggest substantial commonality of the variation of TC activity across the North Atlantic.

Figure 7 shows the percentage of ACE as a function of MJO phase, normalized by time spent in each phase, for each subsector[6] for observations and for the T382 CFS model. The MJO influence on ACE in the different subsectors is somewhat similar to that for the overall basin, with greatest activity in phases 1 and 2 and least

[6] The northeast subsector is not shown because it has relatively little TC activity.

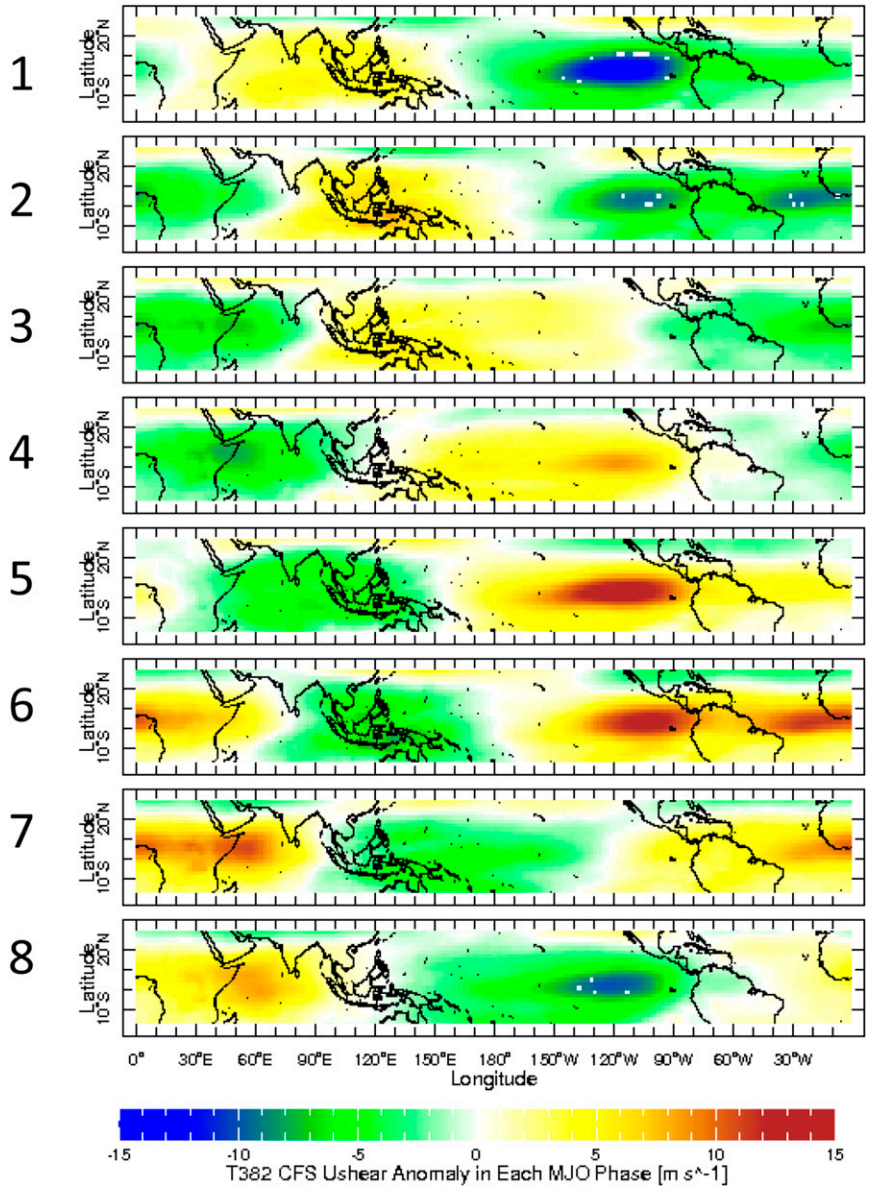

FIG. 6. Anomalous 200–850-hPa zonal wind shear ($m\,s^{-1}$) in the T382 CFS model during the days of each of the model's eight MJO phases during May–November of 1981–2008. Anomalies are defined with respect to the model climatologies covering the 28 years for each of the 214 days in the 7-month season. Anomalies are for the vector shear and not the shear magnitude (see text).

activity in phases 6 and 7. Subsector deviations from this general pattern are greater in the observations than in the model. However, visual examination of Fig. 7 shows, for observations, peak percentages during MJO phase 2 for the Caribbean, Gulf of Mexico, and eastern U.S. subsectors—all in the western portion of the basin, and peak percentages during phase 4 for the north-central and southeastern subsectors—both farther to the east. Although phase 4 is not a time of generally enhanced North Atlantic TC activity, a west-to-east propagation of TC activity is nonetheless roughly suggested, possibly related to the propagation of the MJO. In the T382 CFS model, peak activity in the Gulf of Mexico occurs during a lower MJO phase number (phase 1) than found in the sectors to its east. These suggestions of possible eastward propagation motivate further analysis.

To display the information in Fig. 7 in a maplike format, Table 4 shows, for each subsector and for each MJO phase, the percentage of the average ACE over the 8 MJO phases, in observations and in the model. (Thus,

TABLE 2. Correlation between TC activity in observations and in T382 CFS model over the eight MJO phases, by subsector, and for the total basin (lower-left entry). Top entry is for number of TCs, bottom entry for ACE. The positions of the cells approximate the locations of the subsectors (see Fig. 2). Correlations significant at the 5% level (two sided, ≥0.74) are shown in bold.

	Gulf	Eastern United States	North-central	Northeast
TC No.	0.62	0.71	**0.75**	0.64
ACE	**0.76**	**0.86**	0.71	0.73
	Total basin	Caribbean	South-central	Southeast
TC No.	0.71	0.06	0.36	0.34
ACE	**0.87**	0.28	0.61	0.22

TABLE 3. Correlation between ACE in each subsector and ACE in Atlantic basin as a whole, over eight MJO phases, for observations and CFS T382 model.

	Obs	CFS T382 model
Gulf of Mexico	0.74	0.80
Caribbean	0.75	0.19
Eastern United States	0.90	0.98
South-central	0.84	0.97
North-central	0.77	0.87
Southeast	0.52	0.99

the eight-phase average for any subsector is 100.) The left side of Table 4 shows the percentages of average in the observations and the right side the T382 CFS model. For MJO phase 1, a phase having overall high TC activity, both T382 CFS and observations have above-average ACE in the Gulf of Mexico and in the eastern U.S. subsector, as well as the south-central subsector where many TCs form or traverse on their journey toward North America. Some of the eastern sectors are not more than the expected average in phase 1 in the observations, but all sectors are above average in the model. Before examining Table 4 in more detail, let us consider the idea that if subsector preferences (including those related to eastward propagation) exist in nature, one would hope that the model would reflect them as found in the observations. The degree of similarity of the pattern of subsector details in the observations versus the T382 CFS model is provided in Table 5, which shows, for each phase, the spatial (over the seven subsectors) correlation of the observed versus model percentages of average for both ACE and additionally for TC number.[7] During phase 1, the model and observations show significantly well correlated spatial patterns of percentages for ACE, with 0.84 correlation. Although model and observed spatial patterns are positively correlated in all MJO phases except for phase 2, most of the correlations are not statistically significant, indicating that any MJO-related propagation of enhanced TC activity within the Atlantic basin, if existent, is not necessarily well reproduced in the model. However, the reality of such propagation still needs a more convincing demonstration in the observations and/or the model, and we return to Table 4.

Table 4 shows that, in observations, the greatest percentages of average are in the westernmost subsectors in phase 2, in the more central subsectors in phase 3, and in the easternmost subsectors in phase 4. A similar west-to-east movement is suggested in the model between phases 1 and 4 but does not appear as clearly. To describe such propagation more quantitatively, the centroid of the location of all TC activity is shown as a function of MJO phase for both observations and the T382 CFS model in Fig. 8, for TC number and for ACE. These plots show, first, that the model TCs tend to occur about 6° farther south, and nearly 10° farther east, than those in nature. This southeast displacement has been suggested above (Table 1, Fig. 3) and was found at least partly attributable to biases in large-scale environmental fields (Figs. 4–6). Aside from this general model bias, both model and observations show a tendency toward west-to-east propagation of the centroid position of TC number and ACE between MJO phases 1 and 4, with a return to the west during MJO phases 5–8, which have lower overall TC activity. A nonrandomness of the zonal migration is suggested more clearly when considering the changes between centroids two MJO phases apart (e.g., phase 1 versus 3, then 2 versus 4, etc.) or between running averages of the centroids of two consecutive phases (e.g., phases 1 and 2, then 2 and 3, etc.), either of which remain consistently eastward for the lower phase numbers and then consistently westward during the higher phase numbers, in both observations and the model, and for both TC number and ACE. That is, in all cases, there are just two changes in the centroid's zonal direction (for the two-phase-apart direction, or the running mean direction) over the course of the eight MJO phases. While this may seem significant, the probability of only two direction changes in a sequence of eight opportunities in a random environment is 0.22, so the evidence for eastward propagation can be considered only suggestive. However, if it appears in several models, or appears more smoothly in a larger sample of observations, a stronger case for MJO-related subsector propagation may be possible.

One reasonably might ask what physical mechanisms could cause TC activity to propagate eastward during MJO phases 1–4, and westward during phases 5–8, when

[7] Because this correlation is computed over only seven subsectors, a correlation of 0.80 is required for statistical significance at the 5% level for a two-sided test.

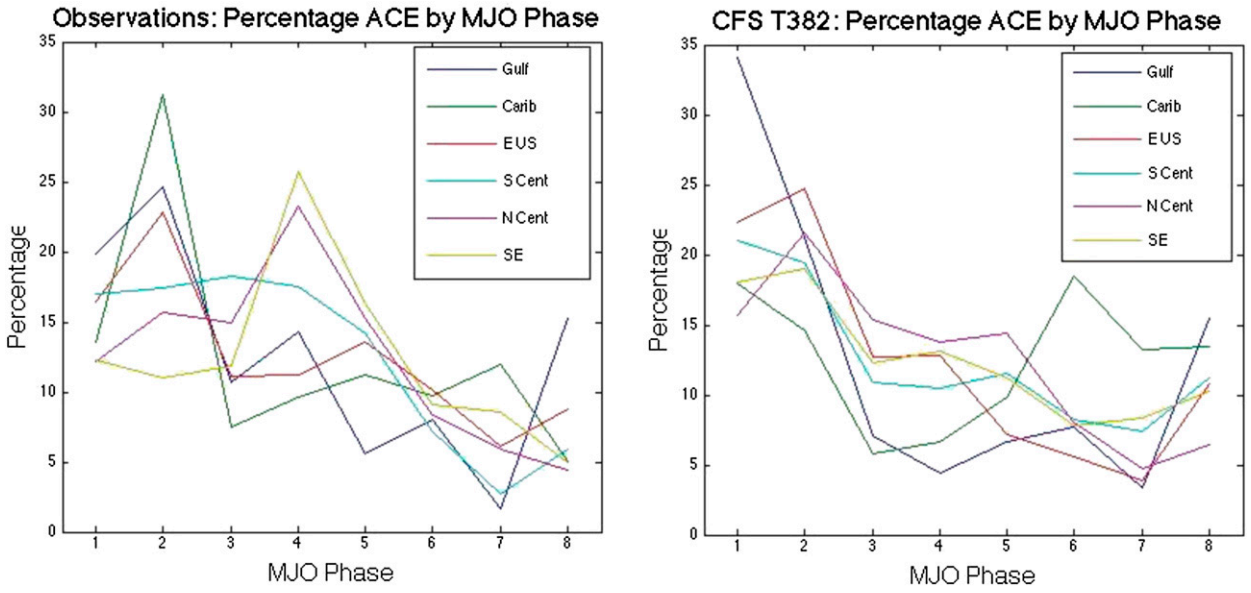

FIG. 7. Percentage of ACE in six subsectors (see Fig. 2) as a function of MJO phase for (left) observations and (right) the T382 CFS model. ACE is normalized by the differing amounts of time spent in each MJO phase. All lines average 12.5% across the eight MJO phases.

the convectively active MJO itself traverses the Atlantic fairly quickly during phases 8 and 1. One possible explanation is that, within any MJO phase, many of the TCs begin with convection associated with easterly waves, which, possibly along with their attendant equatorial Rossby waves (Matthews 2000), move westward at low latitudes while the MJO propagates eastward. There may be a delay of one or more weeks between the time of most active genesis and growth and the time of the maximum activity level of the basin. It is also possible that Africa remains in a convectively enhanced state following the MJO passage, resulting in stronger and more frequent easterly waves moving from Africa into the eastern Atlantic, subsequently undergoing tropical cyclogenesis as they travel westward in the eastern part of the MDR. These ideas require further research.

While the cyclical migratory behavior of TC activity within the North Atlantic basin may be weakly physically related to the MJO rather than purely sampling variability (despite failing to be statistically demonstrated here), the fact that the centroid of TC activity spans only 6°–8° of longitude may imply limited practical consequences for predicting MJO-related subbasin preferences for TC activity.

b. CFSv2

1) MJO PREDICTION AND BASINWIDE MJO INFLUENCE ON TCS

While the T382 CFS is a good vehicle for exploring the potential for more detailed TC predictions, the standard-resolution (T126) version of CFSv2 is currently used in NOAA's actual forecast operations. For the CFSv2, 45-day runs are initialized four times daily on each day of each year during 1999–2010, allowing for not only analyses of TC activity relative to the MJO state, but also an assessment of the skill of the model (against observations) in predicting MJO behavior and TC activity out to 45 days at all times of the year. The MJO state is defined using the method of Wang et al. (2014), using harmonic analysis and a bandpass filter. Observations are taken from the corresponding CFS Reanalysis data (Saha et al. 2010). Here, the forecasts from each of the four times each day are used as individual "ensemble members" for the MJO forecast starting from each day.

An initial issue to probe with CFSv2 is the fidelity of the model in predicting the observed MJO behavior during the first few weeks of lead time. Figure 9 shows the anomaly correlation and RMSE of hindcasts of the two RMM components of the MJO as a function of target month and lead time. These results match well with those in Wang et al. (2014). A feature in common between the two sets of results is the relatively higher skill seen during winter than at other times of the year. These skill results are summarized over all seasons in Fig. 10, which shows anomaly correlation and RMSE as a function of lead time. The decrease of anomaly correlation to 0.5 at a lead time of 20 days corresponds closely with Wang et al. (2014).

Results of diagnostics of systematic error in the model's reproduction of MJO behavior are shown in Fig. 11. The model very slightly underestimates MJO amplitude at

TABLE 4. (top) Location key of seven geographical subsectors. (bottom) The percentage of the average over the eight MJO phases, of ACE in (left) observations and (right) in the T382 CFS model, by the MJO phase for each of the seven geographical subsectors in the North Atlantic. The average entry for any subsector, over the 8 phases, is 100. The location of the cells within each table roughly corresponds to the location map shown in Fig. 2 (e.g., the four entries in the top row are for the Gulf, eastern United States, north-central, and northeast subsectors, respectively). For each MJO phase, the spatial distribution of the percentage of MJO-phase-averaged ACE is highlighted, and the correspondence between observations and the model are revealed. Entries of 130% or greater are shown in bold.

Gulf	Eastern United States Caribbean	North-central South-central	Northeast Southeast	Gulf	Eastern United States Caribbean	North-central South-central	Northeast Southeast
Observations				T382 CFS model			
			Phase 1				
159	**131**	97	70	**273**	**178**	125	**135**
	109	**136**	99		**144**	**168**	**144**
			Phase 2				
196	**182**	126	**154**	**170**	**198**	**172**	**149**
	250	**139**	88		117	**155**	**152**
			Phase 3				
86	89	119	52	57	102	123	92
	60	**145**	95		47	87	99
			Phase 4				
115	89	**186**	**181**	35	102	111	**154**
	77	**140**	**206**		53	84	104
			Phase 5				
45	109	122	**134**	53	58	115	105
	90	114	**130**		78	92	90
			Phase 6				
64	81	68	78	62	45	64	65
	78	57	73		**148**	66	63
			Phase 7				
13	49	47	77	28	31	38	51
	96	21	69		105	59	66
			Phase 8				
122	70	35	54	124	86	51	49
	41	47	40		108	90	82

short lead times (left panel) and shows realistic amplitude at longer leads. The decreasing amplitude of the ensemble mean with longer leads is an expected effect related to partial cancellations due to slightly differing MJO phases among the members. Systematic errors in MJO phase (Fig. 11, right panel) indicate some slowness in phase propagation beginning very quickly after initialization and maximizing at about day 10–12, diminishing just slightly at longer leads rather than continuing to increase. More will be said below about this systematic phase propagation speed error and a design for its statistical correction.

To assess the realism of the CFSv2 model's variation of TC activity as a function of the MJO phase, we compare model hindcasts to observations for the four TC variables (number of TCs, ACE, TC genesis, and TC rapid intensification) as done for the T382 CFS above. The relative frequency of these variables as a function of MJO phase, normalized by time spent in each phase, is shown in Fig. 12 for the observations and the CFSv2. As found for the T382 CFS (Fig. 1), model TC activity is greatest in MJO phases 1 and 2, roughly in keeping with the observations, and relatively lower in MJO phases 6 and 7. The correlations between the model and observed activity over the 8 MJO phases are similar to those found in the T382 CFS—roughly 0.70 to 0.85, except only 0.65 for genesis (see Fig. 12 caption). Although we would like to assess the advantage of the higher resolution in the T382 CFS, differences in the percentage of TC activity per MJO phase in the model versus observations may also come about because of the differing analysis periods (1981–2008 for T382 CFS, 1999–2010 for CFSv2). The longer period covered by the T382 CFS likely better protects its results from sampling error than the shorter CFSv2 period, which may have had regimes easier or harder to predict than those averaged over the longer period.

TABLE 5. Spatial correlation between percentage of MJO-phase-averaged TC activity in the observations and the T382 CFS model over the seven subsectors (i.e., the entries shown in the left vs right sides of Table 4) for each of the eight MJO phases: number of TCs (top row) and ACE (bottom row). Correlations significant at the 5% level (two sided, ≥0.80) are shown in boldface.

	Phase							
	1	2	3	4	5	6	7	8
TC No.	**0.86**	−0.27	0.10	0.71	**0.86**	0.46	0.50	0.27
ACE	**0.84**	−0.29	0.44	0.64	0.75	0.20	0.72	0.60

Additionally, the ocean model upgrade from MOM3 to MOM4 may give CFSv2 an advantage.

To help account for differences between the analysis periods covered by the two model versions as a possible cause of the differing results, analyses of the variation of TC activity as a function of the MJO phase are repeated for each model version using only the 10-yr common period of 1999–2008. Results are shown in Fig. 13 for the T382 CFS and for the CFSv2, to be compared with one another and with the observed results shown in the left column of Figs. 1 and 12.[8] Results for T382 CFS differ slightly from those using the 1981–2008 period and indicate mainly a slightly lower correspondence to the observed percentages. Meanwhile, results for CFSv2 are essentially unchanged from those for 1999–2010 but also lead to a very slightly lower correspondence to the observed percentages.

A comparison between the common period results places the two model versions roughly equivalent in their correspondence with the observed normalized percentage distribution of TC activity among the MJO phases, although CFSv2 results appear slightly more favorable (Table 6). However, the CFSv2 runs are initialized continuously throughout the season, while T382 CFS is initialized only once in late April and hence is mainly a free run over the course of the hurricane season. Although the continuous initialization might provide an advantage to the CFSv2 forecasts only during the first two weeks of the runs, it may be sufficient to offset a possible advantage of the higher resolution in T382 CFS. While an analysis of the two model versions only for the late April start time would eliminate the effects of this design difference, there is too little TC activity during May and early June to provide a meaningful comparison. The question of the benefit of increased resolution therefore remains unanswered.

Acknowledging that the result for CFSv2 (Fig. 12) compared with T382 CFS (Fig. 1) may be related to an unknown combination of the differing model analysis periods (with unknown effect), the model resolution difference (possibly to the benefit of T382 CFS) and the model initialization design (likely to the benefit of CFSv2), and the ocean model difference (to the benefit of CFSv2), we still can say that the observed relationship between MJO and TC activity is approximately reproduced in both the T382 CFS and CFSv2 model versions.

The geographical distribution of the ACE over the tropical and North Atlantic for the CFSv2 model is shown in Fig. 14 for MJO phase 2 (a phase of high activity) and phase 7 (a phase of low activity). Although the difference in model activity between the two MJO phases is seen to be in the correct sense (greater activity in phase 2 than phase 7) and the locations of the observed activity are also fairly well reproduced, some differences are noticeable. For example, in both phase 2 and phase 7, a larger proportion of the activity occurs in the 10°–20°N latitude band in the model than in observations. Although detailed analyses of the model's environmental fields is not undertaken as it was for the T382 CFS, the general tendency for more activity to the south and southeast is reminiscent of similar findings in T382 CFS. This similarity is not surprising, given that the two model versions have dynamical similarities, especially in the atmospheric components.

Previous studies have indicated a slowness of the CFS model MJO propagation, particularly when the convective phase is passing through the vicinity of the eastern Indian Ocean and Indonesia (Wang et al. 2014). Wang et al. (2014) attribute the model slowness to slowness in the convection response to the large-scale anomaly fields (e.g., moisture, vertical shear, pressure) in regions requiring MJO reamplification (e.g., eastern Pacific, Atlantic, Africa). By contrast, the convection response and thus MJO propagation are at realistic speed in regions involving more straightforward eastward propagation, such as after reamplification over Africa, western Indian Ocean, or western or central Pacific following passage over Indonesia. Here we analyze the overall correspondence of the model versus observed propagation speed by determining the lag that maximizes the lag correlation between forecast and observed MJO phase for each of several forecast lead times. In the absence of any systematic error in phase speed, a zero lag correlation (the correlation for corresponding times for forecast and observation) is expected to be the maximum correlation. If the model's MJO phase speed is lower than that of the observations, the

[8] To get the most robust estimate of the observed normalized percentages of TC activity per MJO phase, the period of 1979–2012 is used, regardless of the model analysis period. When the 1999–2008 period is used for the observed percentages, the correspondence with the 1999–2008 model results is degraded (not shown), possibly as a result of an increase in sampling variability for the short observed period.

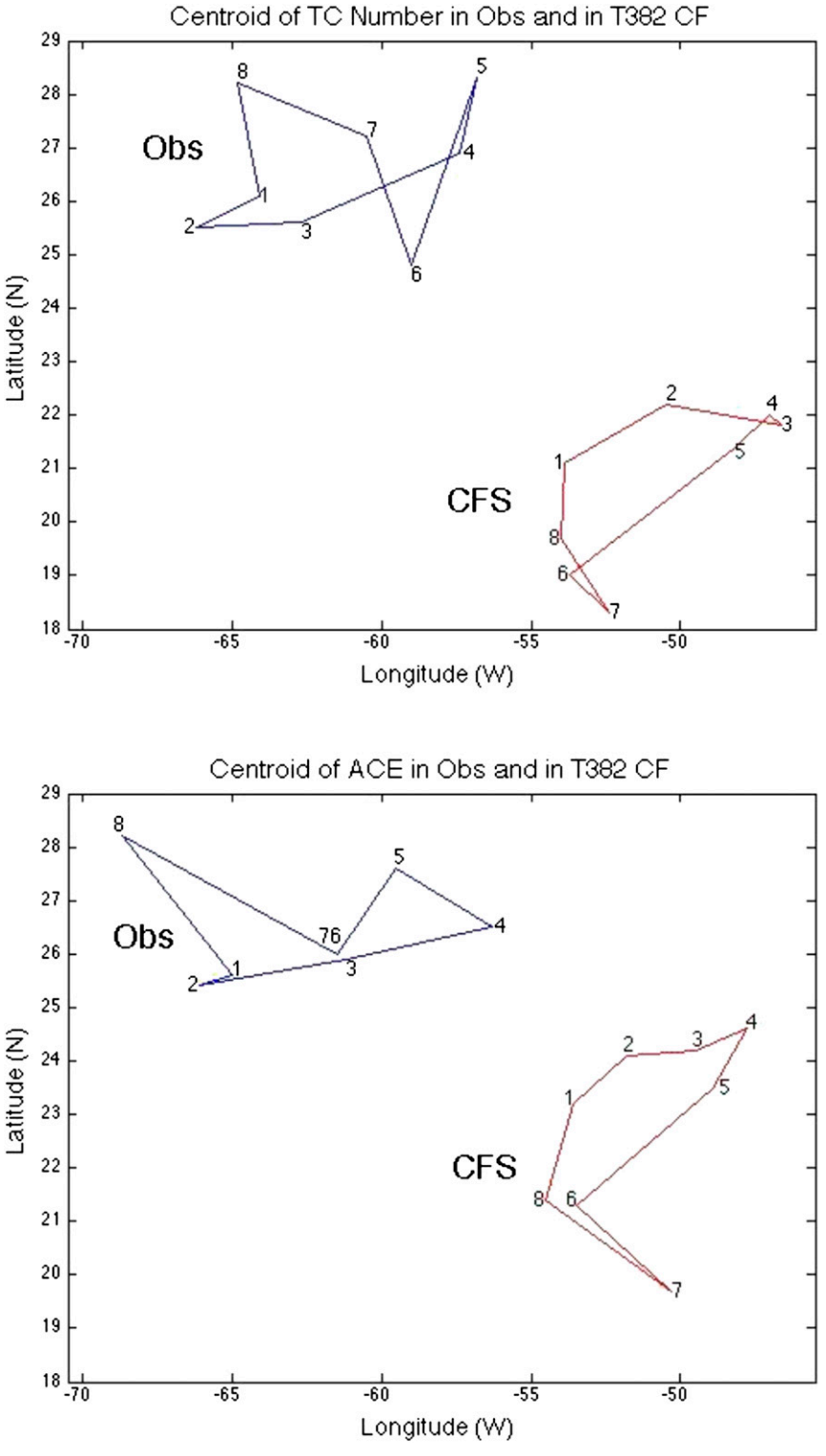

FIG. 8. Location of the centroid of TC activity for each of the eight MJO phases for (top) TC number and (bottom) ACE. Centroid locations are shown in blue for the observations and in red for the T382 CFS model.

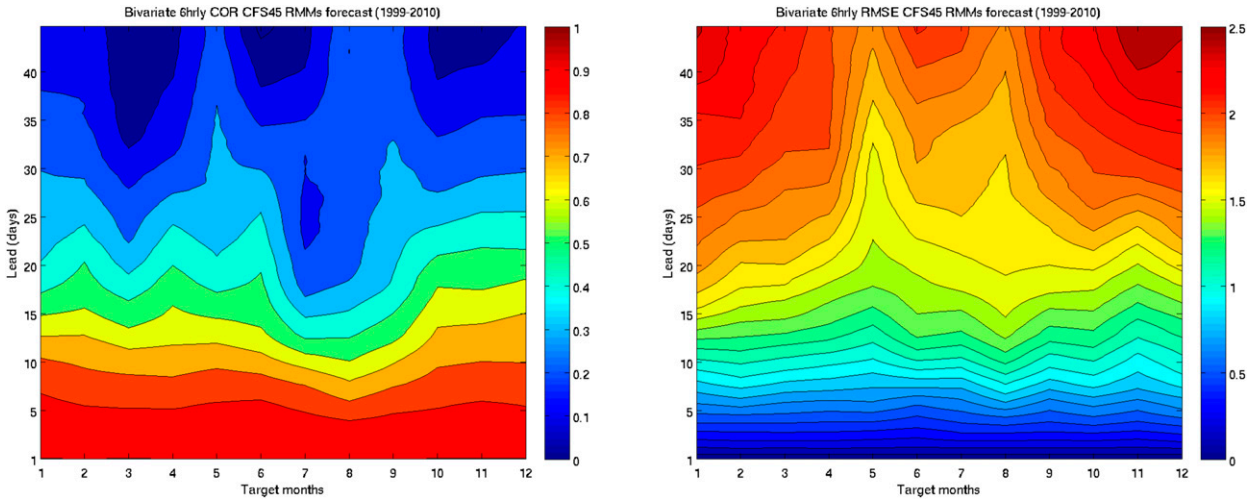

FIG. 9. Verification of MJO behavior (RMM1 and RMM2) in the CFSv2 model initialized four times daily and run to 45 days: (left) anomaly correlation and (right) RMSE as a function of target season (x axis) and lead time (y axis).

correlation would be maximized when the observation is at an earlier time than the model forecast (defined here as a negative lag time). The result of such a lag correlation analysis is shown in Fig. 15. A tendency for slower phase propagation in the model than in observations is noted, as the model lags the observation by approximately 1 day at a 7-day lead. Such slowness of MJO phase propagation is expected to have a degrading effect on the TC forecasts, while elimination of this systematic model error would enable higher-quality model TC forecasts. A statistical correction of the sluggish MJO phase propagation, using regression in a manner similar to that demonstrated in Tippett et al. (2012), would improve skill in MJO forecasts, and a correction of forecasts of a TC variable (e.g., TC number or ACE) is also possible. Because the MJO phase speed bias is not severe, the improvement to the TC forecasts would not be expected to be large but possibly noticeably beneficial.

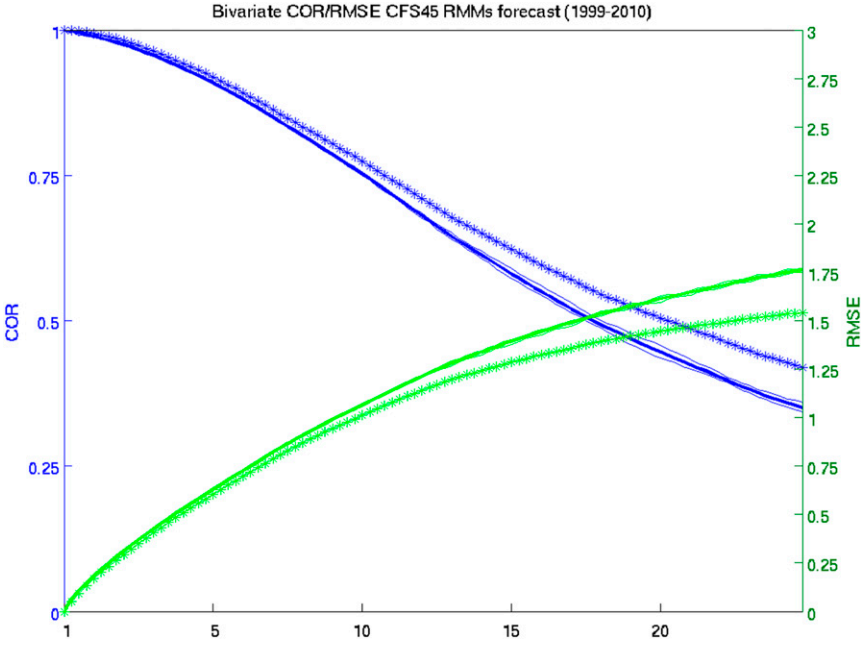

FIG. 10. As in Fig. 9 (correlation and RMSE for CFSv2 MJO behavior), but summarized over all seasons as a function of lead time out to 25 days for the mean of the individual ensemble members (lower skill lines, solid) and for the ensemble mean (higher skill lines, asterisks).

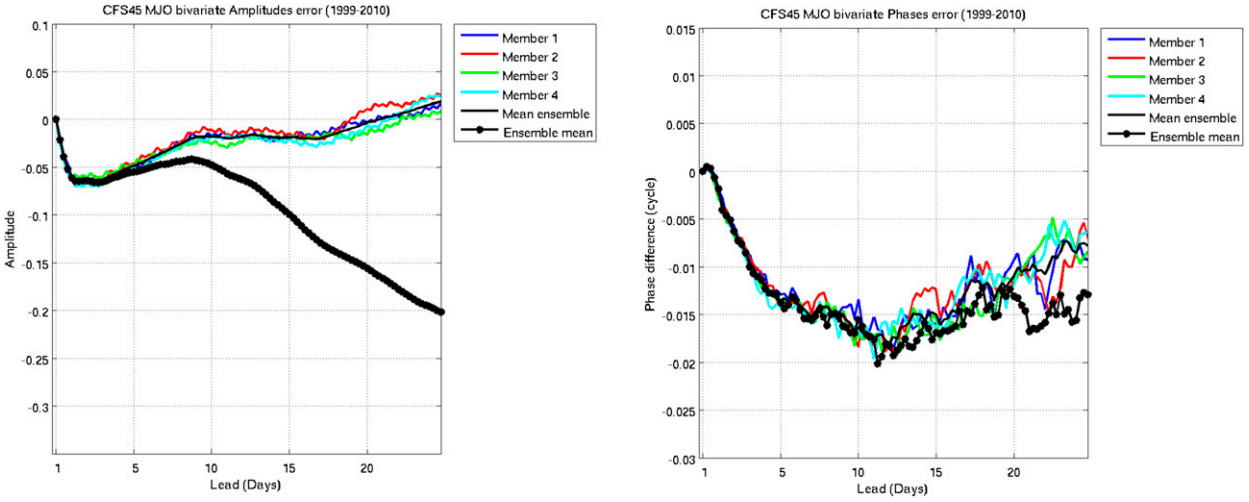

FIG. 11. Diagnosis of systematic errors in (left) amplitude and (right) phase in CFSv2 MJO behavior. Results are shown for both individual ensemble members and the ensemble mean.

2) SEASONAL AND INTRASEASONAL PREDICTIVE SKILL FOR TC ACTIVITY

The usable levels of skill in predicting the MJO amplitude and phase out to 2–3-week lead time, combined with the approximately realistic relationships between MJO phase and TC activity in the North Atlantic basin, would be expected to lead to CFSv2-predicted intraseasonal fluctuations of Atlantic TC activity bearing resemblance to those observed. To assess the degree to which such an expectation is realized, the skill of the CFSv2 45-day hindcasts is evaluated over the 1999–2010 period. Figure 16 shows time series of TC number over the Atlantic basin for the 2000 and 2003 storm seasons as examples of a relatively ''skillful'' and ''unskillful'' years, respectively, for CFSv2 forecasts, compared to the observed TC number from the NHC Best Track HURDAT. Results are shown for lead times for the first week through the fourth week. The CFSv2 forecasts for each day are a 20-member ensemble comprising the four daily forecasts for the 5 days prior to the first forecasted day. Skills are higher for year 2000 at all lead times (on average, ~0.8) than 2003 (~0.7). Although skill decreases with increasing lead time in both years, skill is still at moderately high levels even for the third and fourth week.

While one of the contributions to positive correlations in the forecast versus observed time series in Fig. 16 is from correctly predicted variations within the season, the general reproduction of the seasonal cycle itself is also a large contributor. To isolate the level of skill in reproducing the week-to-week anomaly variations within the season, part of which is assumed related to the MJO influence, we subtract the climatological seasonal cycle, based on the 1999–2010 period, from the storm counts. Figure 17 shows the resulting time series of anomalous storm counts in the forecasts and observations for 2000 and 2003 seasons in similar fashion to Fig. 16 for total storm counts. It is noted that intraseasonal variability is reproduced well in week 1 in 2000, with a correlation skill of 0.61, and drops to 0.22 in week 2. Beyond week 2 the model shows no discernible skill. In year 2003 the skill is near zero for forecasts at all leads. The correlation results for other years (not shown) vary between the levels shown for 2000 and 2003 with an average week 1 correlation of 0.38 and week 2 correlation of 0.19.

To analyze more closely the intraseasonal predictive skill for anomalous TC activity, we compute correlations between forecast and observed activity for each year and for all 12 years collectively. To help reduce the expected sampling error for the 12-yr sample of years, the climatology of observed TC activity is computed for each day between May and November, pooling the 5 days centered on the day in question. Figure 18 shows correlations between CFSv2 forecasts and corresponding observations for TC number for each year for five lead time categories: 1–3, 4–6, 7–9, 13–15, and 19–21 days. Integrated correlations over all years are shown for each lead time by labels on the right side of the plot. Results indicate moderately high skill—between 0.6 and 0.8 for most years—for the 1–3-day predictions, with progressively decreasing skills with increasing led time. At 2-weeks lead, average correlations fall below 0.3, a level sometimes used to distinguish ''usable'' from nonusable forecast skill (O'Lenic et al. 2008).

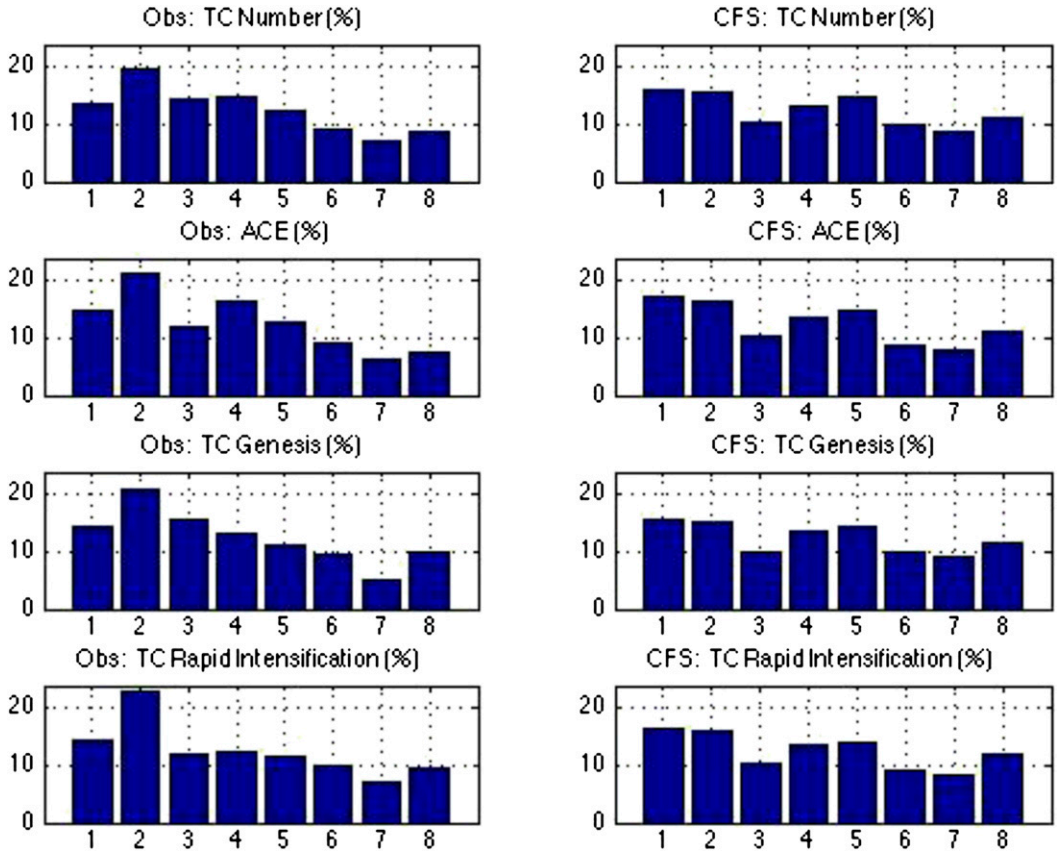

FIG. 12. Percentage distribution of Atlantic hurricane activity by MJO phase for (left) observations and (right) CFSv2 model for (top) number of storms, (second from top) accumulated cyclone energy, (second from bottom) storm genesis, and (bottom) instances of rapid intensification. The data are normalized by time spent in each MJO phase. Correlations between the observed and model patterns over the eight MJO phases are 0.73, 0.83, 0.65, and 0.76, respectively.

The same analysis applied to ACE yields results as shown in Fig. 19, which are similar except that slightly higher general skill levels are indicated for forecasts of ACE as compared with TC number. This result is consistent with the relative skill ranking noted earlier for reproduction of the observed relationships between MJO phase and TC activity in the T382 CFS (section 3a). Both model versions' outcomes are consistent with past findings (e.g., Klotzbach 2010, among others). The higher skills for ACE may be due to more graduated and integrative nature of ACE as compared with the more binary and discrete TC number and the consequent lower sensitivity and lesser statistical robustness in the latter variable. Higher ACE skill may also be due to the larger influence of integrated TC intensity, as implied by Klotzbach (2012) for cases of rapid TC intensification.

We conclude that there is a moderate amount of predictive skill for Atlantic TC activity during the first week, a small amount for the second week, and close to no skill from the third week onward. This skill decay rate closely resembles that found in the statistical prediction results in Slade and Maloney (2013), where MJO predictions were helpful in predicting Atlantic TCs up to 2 weeks' lead time. The approximately correct predictions of the MJO phase and amplitude, and its influence on TCs as noted earlier, are most likely contributing factors to the positive skills in predicting the intraseasonal fluctuations in TC activity.

4. Discussion

The Madden–Julian oscillation (MJO) is known to exert some control on North Atlantic tropical cyclone (TC) activity from week to week within any hurricane season. To explore the possibility of better TC predictions based on forecasts of MJO behavior, we analyze retrospective hindcast data on the MJO and on TC activity in two versions of NOAA's Climate Forecast System (CFS) coupled ocean–atmosphere model. One version is the current operational CFSv2 at T126 horizontal

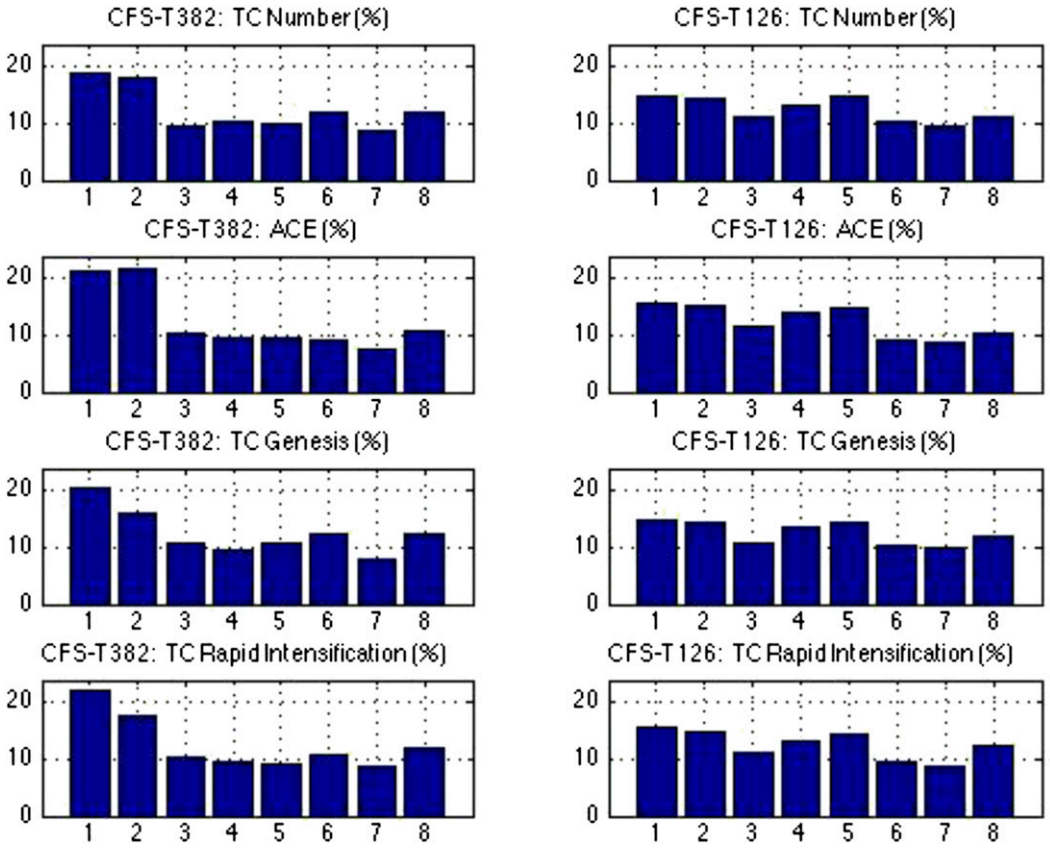

FIG. 13. Percentage distribution of Atlantic hurricane activity by MJO phase for (left) T382 CFS and (right) CFSv2 model, each run only over the common period of 1999–2008. Percentages are shown for (top) number of storms, (second from top) accumulated cyclone energy, (second from bottom) storm genesis, and (bottom) instances of rapid intensification. The data are normalized by time spent in each MJO phase. Correlations between the model and observed patterns over the eight MJO phases for the four TC variables for T382 CFS are 0.55, 0.71, 0.55, and 0.66, respectively. For CFSv2 the comparable correlations are 0.71, 0.84, 0.57, and 0.70.

resolution, and the other is a high-resolution version of the CFS at T382 resolution. The analyses seek evidence about the degrees to which each CFS version reproduces reality in terms of 1) reproducing and/or predicting the MJO and 2) reproducing the observed relationships between the MJO phase and TC activity. Because the operational CFSv2 is initialized four times daily during the 1999–2010 period, we are able to verify the quality

TABLE 6. Correlation (top number in any cell) and root-mean-square error (bottom number in cell) between percentage distribution of four types of TC activity (in columns) across the eight MJO phases in a model version vs the observations. Results for the T382 CFS are shown in top rows, CFSv2 in bottom rows for each of two analysis periods: the model version's own period and the common period of 1999–2008. The last column shows an integration of the results over the four TC activity types, whose values are squared, summed, divided by 4, and square rooted.

Model version	Analysis period	TC No.	ACE	Genesis	Rapid intensification	Integrated TC activity
T382 CFS	1981–2008	0.71	0.87	0.52	0.76	0.73
		2.7	2.4	3.9	3.0	3.1
T382 CFS	1999–2008	0.55	0.71	0.55	0.66	0.62
		3.6	3.8	3.9	3.7	3.8
CFSv2	1999–2010	0.73	0.83	0.65	0.76	0.75
		2.6	2.7	3.4	2.9	2.9
CFSv2	1999–2008	0.71	0.84	0.57	0.70	0.71
		2.8	2.8	3.6	3.3	3.1

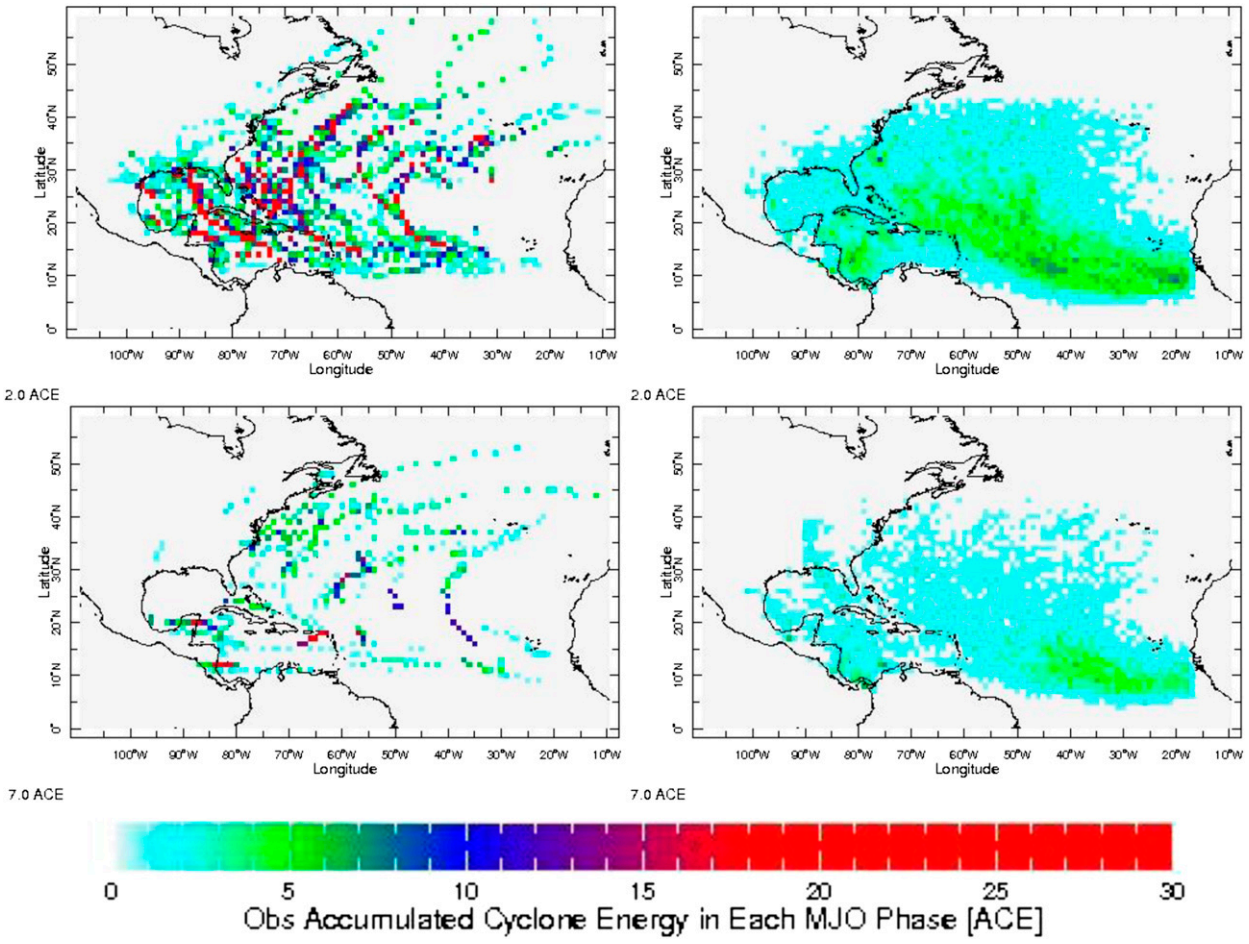

FIG. 14. Atlantic tropical cyclone activity, represented by storm ACE in (left) the observations and in (right) the CFSv2 model. ACE (top) during phase 2 of the MJO, and (bottom) during phase 7 of MJO. Cyclone energy is accumulated not over the lifetime of a TC but, rather, for each grid cell during the given MJO phase. CFSv2 is initialized four times daily through season; leads 1–23 days are included in the analysis. The analysis covers the period of 1999–2010.

of its Atlantic TC activity directly during these years to confirm that its skill in predicting the MJO and its influence on TC activity translates into skill in predicting TC activity. By contrast, the T382 CFS is initialized only in late April of each year, providing free runs that allow only diagnostics of the relationships between the model's MJO behavior and its TC activity.

Both versions of CFS reproduce MJO behavior realistically and also approximately reproduce the observed relationships between MJO phase and TC activity. In the T382 CFS, there is a weak suggestion of propagation of enhanced TC activity from west to east within the Atlantic basin during MJO phases 1–4, as also noted in the observations. However, such TC propagative behavior appears to span only about 6°–8° of longitude, making application to forecasting subsector TC activity preferences questionable. This possible propagative behavior is outweighed by the more general tendency for MJO phases 1 and 2 to enhance TC activity and phases 6 and 7 to suppress activity over the entire basin.

A detailed view of the TC activity in the T382 CFS indicates a general bias toward too little activity along the East Coast of the United States, in the Gulf of Mexico, and the Caribbean, and too much activity in the southeastern portion of the North Atlantic. This bias appears more prominently during the MJO phases conducive to greatest TC activity (e.g., phases 1 and 2). The bias is found to be related to the model's vertical wind shear climatology, which is stronger than observed over eastern North America and the western subtropical North Atlantic, serving to unduly suppress model TC activity in the western and especially southwestern part of the study domain. The T382 CFS is found to have an eastward shift of the climatological upper-atmospheric trough position over the continental

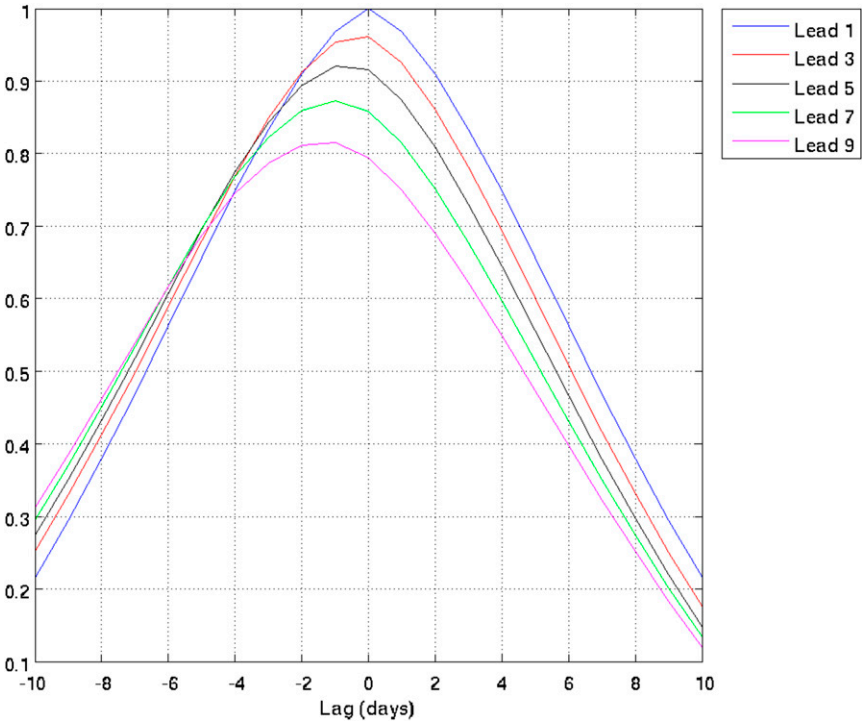

FIG. 15. Diagnosis of ''slippage'' in MJO hindcasts at five lead times. Peak correlations at increasing negative lags with longer lead times indicate a more slowly propagating MJO in the CFS model forecasts than observed.

United States, causing storm trajectories to curve northward and then northeastward over the open ocean rather than reaching locations farther west before curving. In an examination of the observed OLR anomalies as a function of MJO phase, and the corresponding T382 CFS model version of OLR and vertical zonal wind shear anomalies (Figs. 4, 5, and 6), the model is found to reproduce the observed OLR anomaly pattern roughly correctly, but slightly displace the enhanced convection toward the southeast North Atlantic during MJO

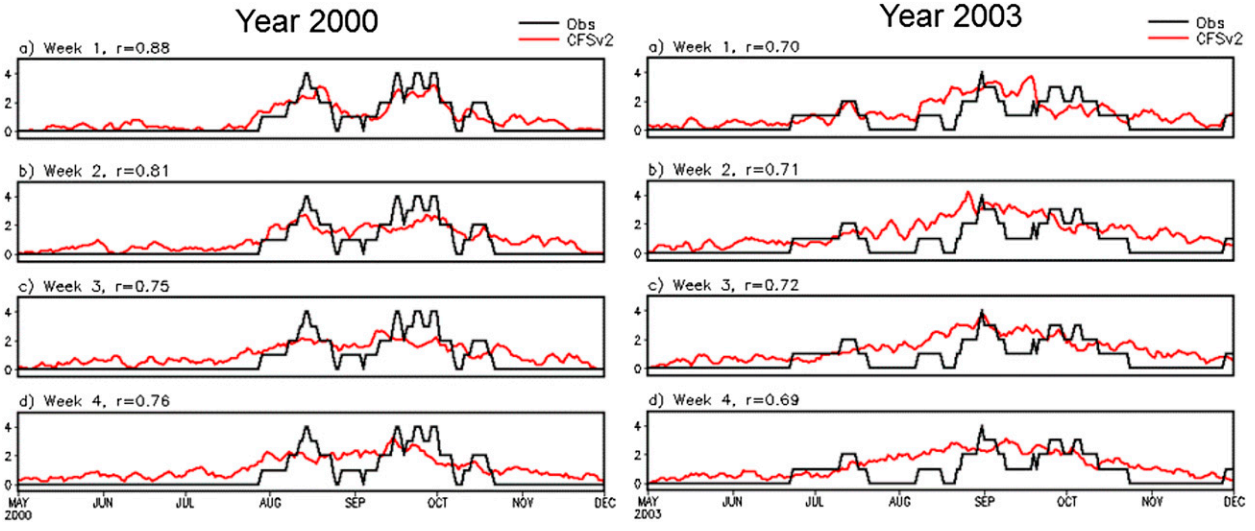

FIG. 16. Time series of TC number over the Atlantic basin for the 2000 and 2003 storm seasons. The forecasted TC number (red) for week 1–4 are compared to observed TC number (black) from the NHC Best Track HURDAT. Correlation scores between the forecasts and observations are indicated above each panel.

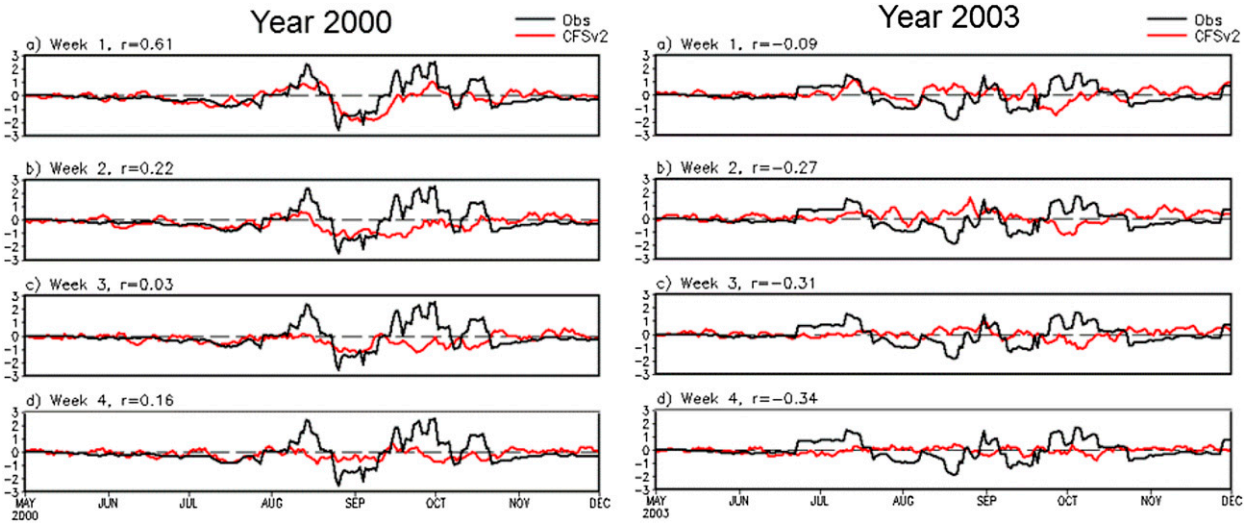

FIG. 17. As in Fig. 16, but for anomalous TC number over the Atlantic basin for the 2000 and 2003 storm seasons. Anomalies are defined with respect to the 12 years of study for the date within the TC season.

phases 1 and 2. Analyses of vertical zonal wind shear anomaly show the northern boundary of the decreased shear during the TC-active MJO phases positioned farther south than the observed northern boundary, creating a model environment less conducive to the longevity and long track length of storms generated to the southeast, moving along a northwestward trajectory.

The operational CFSv2 shows useful skill (correlation of 0.5 or greater) in predicting the MJO phase and amplitude out to approximately three weeks. A systematic

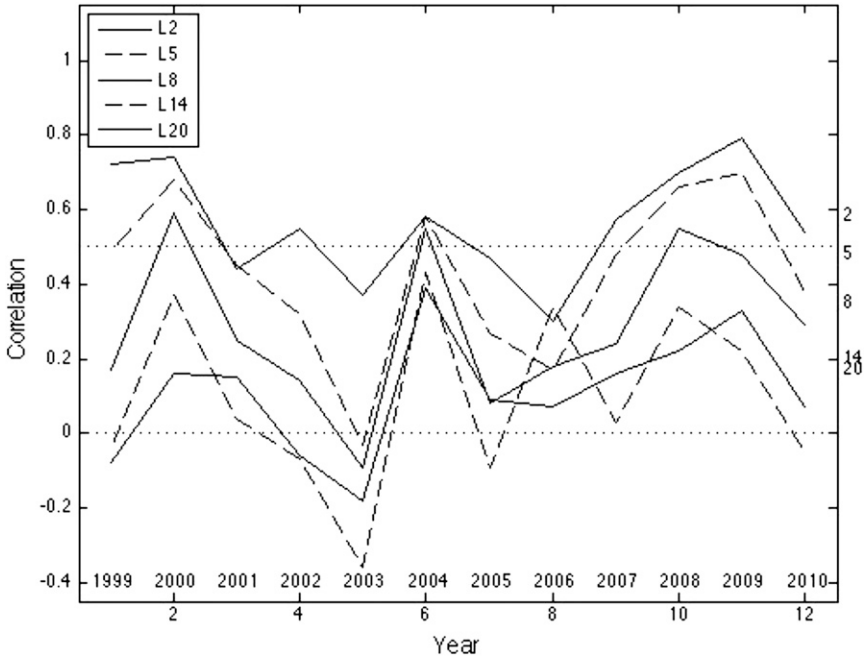

FIG. 18. Correlation between CFSv2 forecasts and observations of variations of the anomalous number of TCs within the 7-month (May–November) TC season of each year from 1999 to 2010. Results for five lead times are shown, including 1–3-day (called L2), 4–6-day (L5), 7–9-day (L8), 13–15-day (L14), and 19–21-day (L20) leads. The average correlation levels integrated over all 12 years are shown just outside the plot on the right side, labeled by lead category. Dotted guidelines shown at 0 and 0.5 correlation levels.

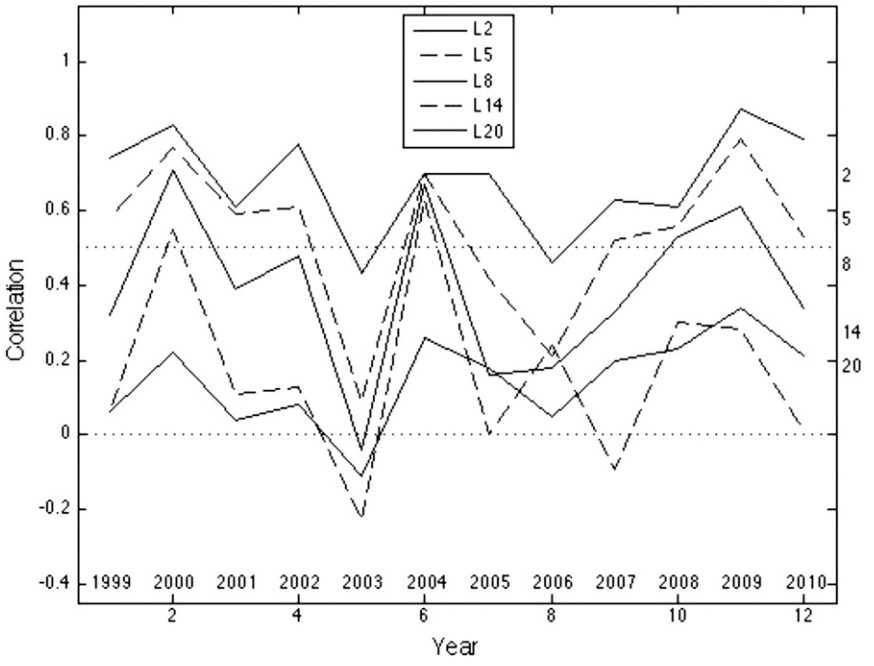

FIG. 19. Correlation between CFSv2 forecasts and observations of variations of the anomalous ACE within the TC season of each year from 1999 to 2010. Format is as in Fig. 18.

error is detected in the CFSv2 in the form of slightly too slow an MJO propagation—a tendency that is correctable using statistical techniques. A conclusion is that predictions of TC activity by CFSv2 do benefit from its MJO predictions (e.g., Figs. 18–19) and that the potential exists for a slightly greater benefit if the systematic error in MJO phase speed were eliminated.

One question raised in this study is whether there is evidence that the higher resolution of the T382 CFS benefits its performance relative to the operational CFSv2. Analyses covering their common hindcast period of 1999–2008 indicate roughly equivalent performance. However, the CFSv2 runs are initialized continuously throughout the season, while T382 CFS is initialized only once in mid-April and hence is mainly a free run over the course of each year's hurricane season. The continuous initialization may provide an advantage to the CFSv2 forecasts sufficient to offset a possible advantage of the T382 CFS's higher resolution. Additionally, the operational CFSv2 has the more advanced MOM4 ocean model, compared with MOM3 in the T382 CFS. Because of these unavoidable experimental design inconsistencies, the question of the benefit of increased resolution remains unanswered.

In conclusion, the operational (T126) CFSv2 and the T382 CFS reproduce MJO behavior fairly realistically and reproduce the MJO's influence on TC activity approximately in keeping with observations despite some overall systematic biases in the spatial distribution of the TC activity. The real-time North Atlantic predictions of TC activity by the operational CFSv2 are therefore believed to be accounting for the MJO phase appropriately, within the 2- to 3-week lead time when MJO is predicted with usable skill.

Acknowledgments. This study was supported by NOAA's Climate Program Office's Modeling, Analysis, Predictions, and Projections Program Award NA12OAR4310076. Most of the authors participated in NOAA's Climate Prediction Task Force.

REFERENCES

Barnston, A. G., M. Chelliah, and S. B. Goldenberg, 1997: Documentation of a highly ENSO-related SST region in the equatorial Pacific. *Atmos.–Ocean*, **35**, 367–383, doi:10.1080/07055900.1997.9649597.

Belanger, J. I., J. A. Curry, and P. J. Webster, 2010: Predictability of North Atlantic tropical cyclone activity on intraseasonal time scales. *Mon. Wea. Rev.*, **138**, 4362–4374, doi:10.1175/2010MWR3460.1.

Camargo, S. J., and S. E. Zebiak, 2002: Improving the detection and tracking of tropical cyclones in atmospheric general circulation models. *Wea. Forecasting*, **17**, 1152–1162, doi:10.1175/1520-0434(2002)017<1152:ITDATO>2.0.CO;2.

Fu, X., and P.-C. Hsu, 2011: Extended-range ensemble forecasting of tropical cyclogenesis in the northern Indian Ocean: Modulation of Madden-Julian Oscillation. *Geophys. Res. Lett.*, **38**, L15803, doi:10.1029/2011GL048249.

Higgins, R. W., and W. Shi, 2001: Intercomparison of the principal modes of interannual and intraseasonal variability of the

North American Monsoon System. *J. Climate*, **14**, 403–417, doi:10.1175/1520-0442(2001)014<0403:IOTPMO>2.0.CO;2.

Jones, C., D. E. Waliser, K. M. Lau, and W. Stern, 2004: Global occurrences of extreme precipitation and the Madden–Julian oscillation: Observations and predictability. *J. Climate*, **17**, 4575–4589, doi:10.1175/3238.1.

Kanamitsu, M., W. Ebisuzaki, J. Woollen, S.-K. Yang, J. J. Hnilo, M. Fiorino, and G. L. Potter, 2002: NCEP-DOE AMIP-II Reanalysis (R-2). *Bull. Amer. Meteor. Soc.*, **83**, 1631–1643, doi:10.1175/BAMS-83-11-1631.

Klotzbach, P. J., 2007: Revised prediction of seasonal Atlantic basin tropical cyclone activity from 1 August. *Wea. Forecasting*, **22**, 937–949, doi:10.1175/WAF1045.1.

——, 2010: On the Madden–Julian oscillation–Atlantic hurricane relationship. *J. Climate*, **23**, 282–293, doi:10.1175/2009JCLI2978.1.

——, 2012: El Niño–Southern Oscillation, the Madden–Julian Oscillation and Atlantic basin tropical cyclone rapid intensification. *J. Geophys. Res.*, **117**, D14104, doi:10.1029/2012JD017714.

Landsea, C. W., and Coauthors, 2004: The Atlantic hurricane database reanalysis project: Documentation for the 1951-1910 alterations and additions to the HURDAT database. *Hurricanes and Typhoons: Past, Present and Future*, R. J. Murname and K.-B. Liu, Eds., Columbia University Press, 177–221.

Madden, R. A., and P. R. Julian, 1994: Observations of the 40–50-day tropical oscillation—A review. *Mon. Wea. Rev.*, **122**, 814–837, doi:10.1175/1520-0493(1994)122<0814:OOTDTO>2.0.CO;2.

Maloney, E. D., and D. L. Hartmann, 2000: Modulation of hurricane activity in the Gulf of Mexico by the Madden-Julian Oscillation. *Science*, **287**, 2002–2004, doi:10.1126/science.287.5460.2002.

Matthews, A. J., 2000: Propagation mechanisms for the Madden-Julian Oscillation. *Quart. J. Roy. Meteor. Soc.*, **126A**, 2737–2651, doi:10.1002/qj.49712656902.

——, 2004: Atmospheric response to observed intraseasonal tropical sea surface temperature anomalies. *Geophys. Res. Lett.*, **31**, L14107, doi:10.1029/2004GL020474.

Mo, K. C., 2000: The association between intraseasonal oscillations and tropical storms in the Atlantic basin. *Mon. Wea. Rev.*, **128**, 4097–4107, doi:10.1175/1520-0493(2000)129<4097:TABIOA>2.0.CO;2.

O'Lenic, E. A., D. A. Unger, M. S. Halpert, and K. S. Pelman, 2008: Developments in operational long-range climate prediction at CPC. *Wea. Forecasting*, **23**, 496–515, doi:10.1175/2007WAF2007042.1.

Saha, S., and Coauthors, 2010: The NCEP Climate Forecast System Reanalysis. *Bull. Amer. Meteor. Soc.*, **91**, 1015–1057, doi:10.1175/2010BAMS3001.1.

——, and Coauthors, 2014: The NCEP Climate Forecast System version 2. *J. Climate*, **27**, 2185–2208, doi:10.1175/JCLI-D-12-00823.1.

Slade, S. A., and E. D. Maloney, 2013: An intraseasonal prediction model of Atlantic and east Pacific tropical cyclone genesis. *Mon. Wea. Rev.*, **141**, 1925–1942, doi:10.1175/MWR-D-12-00268.1.

Tippett, M. K., A. G. Barnston, and S. Li, 2012: Performance of recent multimodel ENSO forecasts. *J. Appl. Meteor. Climatol.*, **51**, 637–654, doi:10.1175/JAMC-D-11-093.1.

Ventrice, M. J., and C. D. Thorncroft, 2013: The role of convectively coupled atmospheric Kelvin waves on African easterly wave activity. *Mon. Wea. Rev.*, **141**, 1910–1924, doi:10.1175/MWR-D-12-00147.1.

——, ——, and P. E. Roundy, 2011: The Madden–Julian oscillation's influence on African easterly waves and downstream tropical cyclongenesis. *Mon. Wea. Rev.*, **139**, 2704–2722, doi:10.1175/MWR-D-10-05028.1.

——, M. C. Wheeler, H. H. Hendon, C. J. Schreck III, C. D. Thorncroft, and G. N. Kiladis, 2013: A modified multivariate Madden–Julian oscillation index using velocity potential. *Mon. Wea. Rev.*, **141**, 4197–4210, doi:10.1175/MWR-D-12-00327.1.

Vitart, F., 2009: Impact of the Madden–Julian Oscillation on tropical storms and risk of landfall in the ECMWF forecast system. *Geophys. Res. Lett.*, **36**, L15802, doi:10.1029/2009GL039089.

Wang, W., M.-P. Hung, S. J. Weaver, A. Kumar, and X. Fu, 2014: MJO prediction in the NCEP Climate Forecast System version 2. *Climate Dyn.*, **42**, 2509–2520, doi:10.1007/s00382-013-1806-9.

Wheeler, M. C., and H. H. Hendon, 2004: An all-season real-time multivariate MJO index: Development of an index for monitoring and prediction. *Mon. Wea. Rev.*, **132**, 1917–1932, doi:10.1175/1520-0493(2004)132<1917:AARMMI>2.0.CO;2.